Eddy covariance carbon flux in a scrub in the Mexican highland

Aurelio Guevara-Escobar[1], Enrique González-Sosa[2], Mónica Cervantes-Jiménez[1], Humberto Suzán-Azpiri[1], Mónica Elisa Queijeiro-Bolaños[1], Israel Carrillo-Ángeles[1], Víctor Hugo Cambrón-Sandoval[1].

[1]Facultad de Ciencias Naturales, Universidad Autónoma de Querétaro, Av. de las Ciencias s/n Juriquilla CP. 76230, Querétaro, Querétaro.
[2]Facultad de Ingeniería, Universidad Autónoma de Querétaro. Cerro de las Campanas s/n Las Campanas, CP. 76010 Querétaro, Querétaro.

Correspondence to: Mónica Cervantes-Jiménez (monica.cervantes@uaq.mx)

Abstract. Arid and sem-iarid ecosystems contain relatively high species diversity and are subject to intense use, in particular extensive cattle grazing which has favoured the expansion and encroachment of perennial thorny shrubs into the grasslands, thus decreasing the value of the rangeland. However, these environments have been shown to positively impact global carbon dynamics. The Moderate Resolution Imaging Spectroradiometer (MODIS) gross primary productivity (GPP) product provides a rapid and broad-scale means for monitoring rangelands, but few studies have validated the performance of MODIS estimates in arid and semi-arid ecosystems. We measured the net ecosystem exchange of C (NEE) with the Eddy Covariance (EC) method and estimated GPP in a thorny scrub at Bernal in Mexico. The hypothesis was that this site might behave as carbon sink. We also tested the agreement with remote sensed GPP estimates from MODIS model. The agreement with EC estimates of two alternative modeling methods were tested: ordinary least squares multiple regression (OLS) or ensembles of machine learning algorithms (EML); the variables used as predictors were MODIS spectral bands, vegetation indices and environmental variables. The Bernal site was a carbon sink despite it is being in an overgrazed condition, the average NEE during fifteen months of 2017 and 2018 was -0.78 g C m^{-2} d^{-1} and the flux was negative or neutral during the measured months. The probability of agreement was higher for the EML (0.6) followed the OLS (0.5) and then MODIS (0.24). We used an EML from a site with similar vegetation and climate to predict GPP at Bernal but the probability of agreement was poor (0.16), indicating the local specificity of this model. Although cacti were an important component of the vegetation the nighttime flux was characterized by positive NEE suggesting that the photosynthetic dark-cycle flux of cacti was lower than ecosystem respiration. The discrepancy between MODIS and EC GPP estimates stresses the need to understand the limitations of both methods.

1 Introduction

Deserts and semi deserts occupy more than 30% of terrestrial ecosystems. Mexico expands almost 2 million km^2 with 50% corresponding to arid and semi-arid ecosystems, mainly the Sonoran and the Chihuahuan deserts (Medrano, 2012). The Spanish-Criollo intrusion (1540-1640) brought new land-use methods, but there is no evidence of additional landscape

degradation from the central highlands to the north-eastern frontier of New Spain until well into the 18th century (Butzer and Butzer, 1997). At the country scale, the extent of grasslands declined and the area of croplands and woody areas increased; being rural-urban migration an important driver of the transition from grasslands to woody vegetation (Bonilla-Moheno and Aide, 2020). The transition from grasslands to shrublands or scrub is linked to the extremely heavy grazing by domestic livestock (Wilcox et al., 2018). The impact of overgrazing is not always fully understood because the many interactions of climate-induced stress with those tied to land use may reduce the resiliency of natural communities (Lightfoot, 2018). To change the environmental degradation trends that Mexico continues to experience, we need to improve the connection at many scales between what scientists know about the functioning of ecosystems and the operation of the economy; engaging policymakers and the support of society at large (Sarukhán et al., 2015). Many other countries are embracing similar efforts.

Vegetation in the arid to semi-arid ecosystems are mostly classified as rangelands. These are one of the most widely distributed landscapes on earth, incorporating a wide range of communities including grasslands, shrublands, and savannah. As rainfall increases in the rangeland the carbon pools and fluxes may be less variable and more responsive to management practices that enhance carbon sequestration (Booker et al., 2013). On the other hand, scrub is a xeric category of shrublands characterized by plants with small leaves, very thorny and its biomass is distributed mainly to roots and leaves rather than the stems (Rzedowski, 1978; Wheeler et al., 2007; Zhang et al., 2017). Commercial value of scrub is low, and because of this under-appreciation, is susceptible to human-caused fire or land use change. Soil erosion and desertification are common consequences of land use change expanding the agricultural frontier, particularly in marginal areas (Mirzabaev et al., 2019). However, the social and institutional constraints to proper range use appear to be greater than the technical ones, including land tenure (Gilles and Jamtgaard, 1982). Therefore, studies based on multiple sources of evidence, considering the driving processes of the land C in Mexico, are needed to aid in policy formulation and to identify regions that may provide important ecosystem services (Murray-Tortarolo et al., 2016).

Substantial biosphere–precipitation feedback is often found in regions that are transitional between energy and water limitation, such as semi-arid or monsoonal regions (Green et al., 2017). A perennial deep rooted woody vegetation, through enhanced evaporation, can increase moist convection and rainfall elsewhere, particularly in the case of a growing season expanding beyond the rainy season (Spracklen et al., 2018). However, global temperature increases may be responsible for changes in plant composition and consequently in the ecosystem hydrology, structure and function in regions such as the Chihuahuan Desert (Lightfoot, 2018). More energy available in the system and consequently changes in the carbon and water cycles are key elements of global warming and oceanic oscillations (Hansen et al., 2015; Piao et al., 2019). This is important for semi-arid ecosystems because vegetation photosynthesis is linked to water availability and, at the same time, most plant species in this environment have evolutionary adaptations to resist prolonged dry spells and also to take advantage of the effects of oceanic oscillations and monsoon rains (Piao et al., 2019; Tang et al., 2012; Zhang et al., 2017). Furthermore, an increase of temperature during the early morning, would decrease relative humidity and consequently condensation or fog; these water inputs are important for many species in arid and semi-arid ecosystems (Bickford, 2016; Males, 2016).

Photosynthesis contributes to carbon sequestration by moving carbon stock from the atmosphere to other pools or sinks, as above ground biomass, roots and soil organic matter (Booker et al., 2013). The role of vegetation in carbon sequestration on arid and semi-arid ecosystems is less evident because the growth rate is low and biomass partition above and below ground is different from that of temperate and tropical forests. The competitive interactions of arid plants at the community level are strongly influenced by rooting architecture and phenological growth (Zeng et al., 2008). Many plants in semi-arid systems support a deep and wide root system as a drought adaptation but also for nutrient uptake (McCulley et al., 2004). Recent time-trends indicate that semi-arid ecosystems regulate the terrestrial carbon sink and dominate its inter-annual variability (Piao et al., 2019; Scott et al., 2015; Zhang et al., 2020). This variability mainly results from the imbalance between two larger biogenic fluxes that constitute the net ecosystem exchange (NEE): the photosynthetic uptake of CO_2 (gross primary production, GPP) and the respiratory release of CO_2 (total ecosystem respiration, R_{eco}). Radiation and water availability are important environmental drivers of NEE and thus, GPP and R_{eco} (Marcolla et al., 2017). However, other carbon fluxes contribute to the imbalance, such as fire and anthropogenic CO_2 emissions (Järvi et al., 2019; Piao et al., 2019) and the atmospheric CO_2 that is inter-converted into soil inorganic carbon in arid and semi-arid ecosystems (Soper et al., 2017); calcium carbonates form at a relatively low rate of 5 to 150 kg C ha^{-1} y^{-1}, but are a carbon sink when they are leached into the groundwater (Lal et al., 2004). The methods used to explore the ecosystems and the understanding of their functioning is changing rapidly, particularly for arid and semi-arid ecosystems (Goldstein et al., 2020; Ma et al., 2020; Xiao et al., 2019; Yao et al., 2020). There are many instruments and techniques for estimating carbon and water fluxes but two stand out in the literature: Eddy Covariance (EC) and remote sensing techniques. EC is a micro-meteorological method that measures the ecosystem community NEE at short time intervals representing a land surface smaller than 1 km^2. The orbital remote sensing measures radiation emitted or reflected by earth surfaces and; using different algorithms, represents different traits of vegetation activity from large scale areas. Both techniques are complementary, but an agreement between their estimates is important for regional, countrywide or global spatiotemporal monitoring of greenhouse gas inventories (Yona et al., 2020), ecological modeling, quantifying the interaction among the vegetation component and the hydrological, energy and nutrient cycles; among others applications (Pasetto et al., 2018). Particularly, products from the moderate resolution spectroradiometer (MODIS) have ample availability and are extensively used to study land surface since 2000.

Gross primary production can be represented by a wide range of models, ranging in complexity from simple regression based on climatic forcing variables to complex models that simulate biophysical and ecophysiological processes (Anav et al., 2015). The MODIS MOD17 product uses a photosynthetic radiation conversion efficiency model (Running and Zhao, 2015), but a better relationship is reported with EC derived GPP when the model uses vegetation indices calculated from the same MODIS platform (Ma et al., 2014; Wu et al., 2010). Although they are black box models in principle, recent modeling efforts report good agreement of GPP estimates obtained from machine learning algorithms or ensembles of models (Eshel et al., 2019; Jung et al., 2019). Different machine learning algorithms are powerful because they can identify trends and patterns in big data sets and solve regression or classification problems.

To generate models of GPP we measured EC fluxes during 2017-2018 in a thorny scrub with semi-arid climate in the highlands of Mexico (Bernal site). Competing models were data-driven machine learning regression ensembles (EML) and ordinary least squares regression (OLS), both using Daymet (Thornton et al., 2017) and MODIS data sets as explanatory variables. The MODIS GPP product was used as a baseline comparison. The second step was to use a EML model based on local data (Daymet and MODIS) from a site with EC instrumentation and similar vegetation to that of Bernal's site and then use that model to predict GPP at the Bernal site. The site we used was Santa Rita from the Ameriflux network. While Santa Rita is in the Sonoran Desert and Bernal is in the southern border of the Chihuahuan desert, both have a similar climate and mesquite vegetation (Figure 1). A good agreement between Bernal EC data and the predictions from Santa Rita model, would support the use of machine learning algorithms as a scale up mechanism. This would be useful to the understanding of rangelands and also improve current earth system models (Piao et al., 2019).

We hypothesized whether or not the semi-arid vegetation at Bernal site was a carbon sink during the wet season or a carbon source during the dry season, since some of the site species reproduce during winter and spring, particularly cacti, *Acacia* and *Prosopis* (Mesquite). Furthermore, the Bernal site had a history of disturbance by overgrazing, this could decrease the GPP and even result in a positive carbon balance; thus being a carbon source. On the contrary, confirming the hypothesis that the shrub vegetation in this semi-arid environment is a carbon sink would contribute to reinforce the reported importance of semi-arid environments in the global carbon balance (Zhang et al., 2020). The measurement campaign presented here was short (March 30 2017 to August 22 2018) but it was not biased by wet winters, since both years were characterized by a less than weak Niño-Niña.

2 Materials & Methods

2.1 Site description

The study site (Bernal) is located at N 20,717, W 99,941 and 2 050 m a.s.l. in the municipality of Ezequiel Montes in Querétaro where real estate development, feedlot beef production, cheese and wine production associated with tourism and, automotive industry development are very attractive options for landowners in the region. Bernal is located in a shallow valley oriented from north to south, approximately 15 to 20 km wide and opening to the south to the Río Lerma basin and then draining into the Pacific Ocean. The northern limit of the valley is surrounded by hill country and its characteristic 433 m in height dacitic dome (Aguirre-Díaz et al., 2013). Moisture-laden winds blow westward from the Gulf of Mexico but the Sierra Gorda, located 60 km east of Bernal, casts a rain shadow over the area (Segerstrom, 1961).

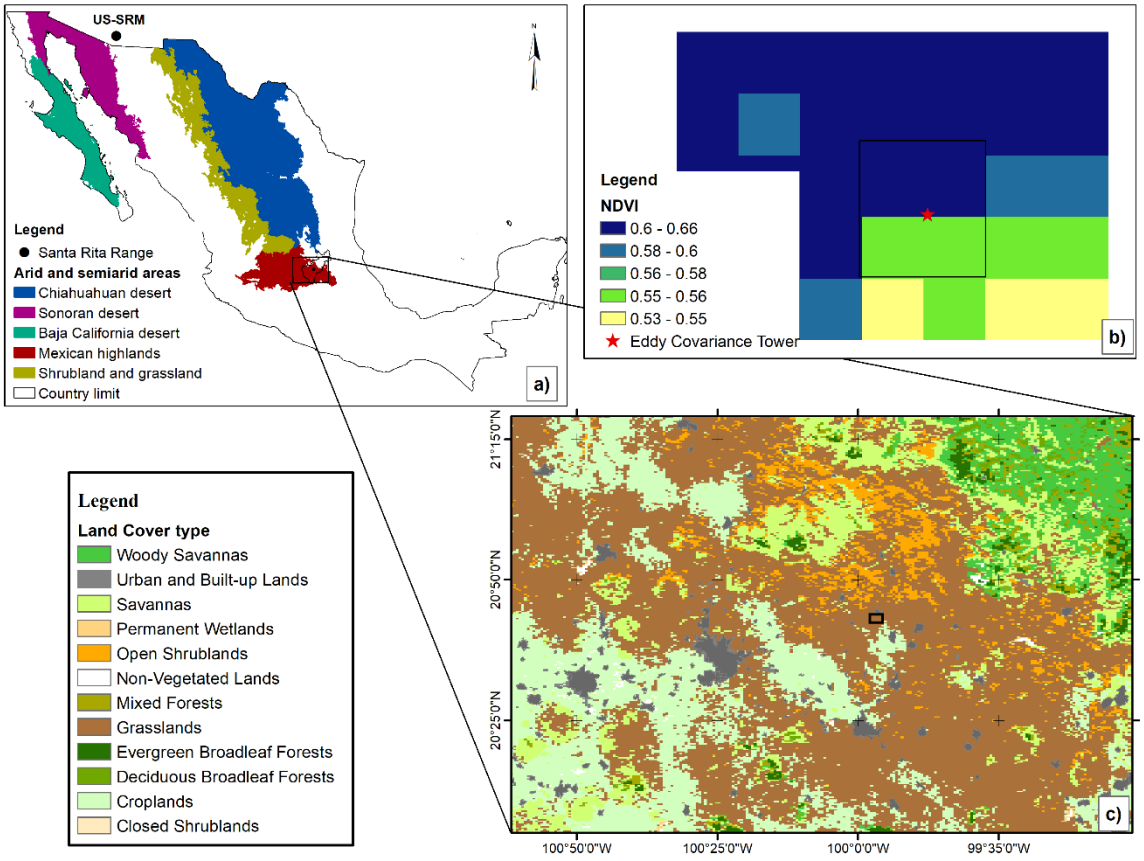

Figure 1. Localization and land use maps for the study site: a) Biogeographic zones of southern North America relevant for the Bernal and Santa Rita sites, the black outline is the state limit for Queretaro b) Heterogeneity of the normalized difference vegetation index (NDVI) surrounding the EC tower at Bernal during the peak of the growing season 2017 (DOY 257), c) Land cover in the region of Bernal site, according to the Annual University of Maryland (UMD) classification (MCD12 MODIS product).

The Bernal site is a private property, with grazing dairy cattle receiving additional concentrated foodstuffs under stall-feeding. We assumed that the footprint of the EC was measuring only the patchy scrub vegetation and the upwind fetch was sufficient; since other vegetation types and surrounding buildings (dairy, yards and poultry housings and ponds) were far away. Grazing was continuous, water for livestock was only available in the feeding and milking area; there were no pasture divisions and the perimeter fence was made of stone. These characteristics of the animal production model and the state of vegetation are representative of land management practices and the scrub vegetation in this region. However, the Bernal site suffered important changes in land use during 2019 and the scrub was suddenly cleared.

The climate is arid with summer rains (BSk), mean annual rainfall is 476 mm and mean annual temperature is 17.1 °C (CICESE, 2015). Prevailing wind is from the east and north-east. The terrain is mostly flat; most grades are below 2%. The soil has a clay loam texture are Vertisols with abundant sub rounded basaltic stones, without rocky outcrops, soil depth is

greater than 0.6 m. The vegetation is less than 3 m in height with an overgrazed herbaceous stratum. The vegetation corresponded to secondary scrub with the dominant genera *Acacia*, *Prosopis* and different Cacti (Figure 2). This site was classified as grassland by MODIS landcover.

For the scrub and tree species, the vegetation importance index (IVI) was determined following Curtis and McIntosh (1950) to assess the vegetation homogeneity. The IVI is the sum of relative dominance, relative density and relative frequency of the species present. For each plant, two stem diameters, the number of individuals (abundance) and identity of each species were measured, as well as the coverage, which is the horizontal projection of the aerial parts of the individuals on the ground, expressed as a percentage of the total area (Wilson, 2011).

Figure 2. Thorny scrub at Bernal, Queretaro during the rainy season 2017. In the foreground *Cylindropuntia imbricata*, a very thorny cactus, shrubs in the background are *Prosopis laevigata* mesquites.

2.2 Eddy covariance measurements

The micro-meteorological EC technique, measures at the plant community level NEE in a non-destructively way, and continuously over time (Baldocchi, 2014). The negative CO_2 fluxes corresponded to NEE, which is equivalent to NEP (net ecosystem production) but with opposite sign. The EC has advantages compared to other techniques that need to scale up measurements from the leaf, plant or soil levels up to ecosystems, especially when the vegetation is heterogeneous (Yepez et

al., 2003). However, EC is an expensive technique, data analysis and processing are complicated, also specific assumptions must be met regarding the terrain, vegetation and micro-meteorological conditions, among other aspects (Richardson et al., 2019).

The fluxes were measured with the EC technique at a height of 6 m with the following instruments: A Biomet system (Licor Biosciences, USA) to measure H_2O and CO_2 fluxes using an IRGASON-EC-150 open circuit analyzer, and a CSAT3 sonic anemometer, KH20 krypton hygrometer, these were connected to a CR3000 datalogger (Campbell Scientific Inc., Logan, UT, USA). The relative humidity and air temperature were measured with an HMP155A probe (Vaisala Corporation, Helsinki, Finland); net radiation was measured with a NR-Lite2 radiometer (Kipp & Zonen BV Delft, The Netherlands); and the photosynthetic active radiation (PAR) was measured with a quantum sensor SKP215 (Skye Instruments, Llandrindod Wells, UK). Measurements of the soils heat flux was implemented with four self-calibrating HFP01SC plates at 80 mm depth and in four representative positions of the landscape (Hukseflux Thermal Sensors BV, Delft, The Netherlands). Three time domain reflectometry probes (TDR) CS616 measured volumetric water content in the ground installed vertically, and two sets of TCAV thermocouples measured the temperature at 60 and 40 mm depths and above the HFP01SC plates (Campbell Scientific Inc., Logan, UT, USA). The TE525 (Texas Electronics, Dallas, TX, USA) tipping bucket rain gauge was installed at 1.2 m high and three meters away from the tower. All these meteorological variables were measured every 5 seconds and average values were stored every 30 minutes; rainfall was accumulated for the same time interval. Sensible (H) and latent (λE) heat fluxes were calculated using the EddyPro package (Licor Biosciences, USA).

2.3 Flux data processing

All EC data were collected at 10 Mhz in the datalogger and reported as μmol CO_2 m^{-2} s^{-1} and processed with the Eddypro package to convert values into average fluxes of 30-minute intervals. Only quality flagged records were used to account for the CO_2 flux (qc_co2_flux = 0) according to the Mauder and Foken (2011) policy in the Eddypro program (Licor, 2019). However, this quality-checking is not sufficient especially in the case of CO_2; therefore, data was post processed using the Reddyproc package of R (R Development Core Team, 2009), to estimate the friction speed thresholds (u*), gap-fill data, and partition the NEE flux into its GPP and R_{eco} components (Wutzler et al., 2018). The filled-in estimates of NEE (NEE_uStar_f), GPP (GPP_uStar_f), and R_{eco} (Reco_uStar) were used from the u* annual base scenario because the difference between the base u* scenario and the 95% u* uncertainty threshold was 0.033 m s^{-1}; only 8.5% of half hour records had a u* below the 95% u* threshold. Only data with a flag equal to 0 was used for the variable NEE_uStar_fqc, as defined by Reddyproc. Carbon dioxide flux data were time integrated and converted to g C m^{-2} d^{-1} using the molar ratio of C. We only reported the continuous measurements of the exchange of CO_2 for the period of April 2017 (DOY 89) to August 2018 (DOY 234) using the EC technique. Due to equipment malfunction and incomplete datasets some periods of time were not considered.

2.4 Remote sensed data

Data was requested via the land processes DAAC AppEEARS to obtain spatial and temporal subsets for the Bernal and Santa Rita sites including: daily surface reflectance (MOD09GA.006 and MODOCGA.006), daily day and night time land surface temperature (LST) (MOD11A1.006 and MYD11A1.006), eight day leaf area index (LAI) and fraction of photosynthetically active radiation (FPAR) (MOD15A2H.006, MCD15A2H.006), sixteen day enhanced vegetation index (EVI) (MOD13Q1.006, MYD13Q1.006), sixteen day gross primary production (GPP) and net photosynthesis (PsnNet) (MOD17A2H.006). Appendix A presents the details of each spectral band of MODIS. Data with less than good quality flags were deleted. Missing data was filled with splines and a database with one day time step was generated, this would smooth linear temporal phenological evolution between any two successive remotely sensed data points (Eshel et al., 2019). Daily accumulated rainfall was requested using the Giovanni GSFC platform (GPM 3IMERGDF.006 and TRMM 3B42.007). Gridded weather parameters from de ORNL DAAC Daymet dataset were: precipitation, shortwave radiation, maximum and minimum air temperature and water vapor pressure. Daymet is a data product derived from a collection of algorithms interpolating and extrapolating daily meteorological observations (Thornton et al., 2017). Following Henrich et al. (2012) and Hill et al. (2006), daily reflectance bands of MODIS were used to compute several vegetation indices: Red Green Ratio Index (RGRI), Simple Ratio (SimpleR), Moisture Stress (MoistS), Disease Stress Index (DSI), Normalized Difference Vegetation Index (NDVI), Normalized Difference Water Index (NDVI_w) and Enhanced Vegetation Index (EVI); the corresponding equations are presented in Appendix A.

2.5 MODIS algorithm for GPP

Estimates of GPP are derived from data recorded by the MODIS sensor aboard the Terra and Aqua satellites. The efficiency (ε, g C MJ^{-1}) with which vegetation produces dry matter is defined as the amount of solar energy stored by photosynthesis in a given period, divided by the solar constant integrated over the same period (Monteith, 1972). Not all incident solar radiation is available for biomass conversion, only about 48% is photosynthetically active (PAR, MJ m^{-2}) and not all PAR is absorbed (Zhu et al., 2008). Thus, carbon exchange is mainly controlled by the amount of PAR absorbed by green vegetation (APAR) and modified by ε (Gitelson et al., 2015). The fraction of absorbed PAR (FPAR) is equal to APAR/PAR, but can be represented by the NDVI spectral vegetation index produced by MODIS (Running 2004). The efficiency term ε is described as the product of different factors as a whole or part of the system (Monteith, 1972), but mostly those related to the efficiencies with which the vegetation intercepts the radiation and the efficiency to convert the intercepted radiation into biomass (Long et al., 2015). The MODIS algorithm that estimates GPP in the MOD17 product is (Running et al., 2004):

$$GPP = \varepsilon * FPAR * PAR, \quad \text{Eq. (1)}$$

$$GPP = \varepsilon * NDVI * PAR \quad \text{Eq. (2)}$$

The ε term in the MODIS algorithm is represented by a maximum radiation conversion efficiency (ε_{max}, kg C MJ^{-1}) that is attenuated by sub optimal climatic conditions, mainly minimum air temperature (Tmin) and vapor pressure deficit (VPD). Two parameters for each, Tmin and VPD, are used to define attenuation scalars for general biome types. These parameters form linear functions between the scalars (Running and Zhao, 2015; Wang et al., 2013): daily minimum temperature at which $\varepsilon = \varepsilon_{max}$ and at which $\varepsilon=0$ and; the daylight average VPD at which $\varepsilon = \varepsilon_{max}$ and at which $\varepsilon=0$. GPP is truncated on days when air temperature is below 0°C or VPD is higher than 2000 Pa (Running and Zhao, 2015). Stress and nutrient constraints on vegetation growth are quantified by the limiting relation of leaf area in NDVI x PAR, rather than constrained through ε (Running et al., 2004).

$$\varepsilon = \varepsilon_{max} * Tmin_{scalar} * VPD\_scalar \quad \text{Eq. (3)}$$

The MOD17 user's guide presents a Biome-Property-Look-Up-Table (BPLUT) with the parameters for each biome type and assumes that they do not vary with space or time (Running and Zhao, 2015). This aspect is important because ε_{max} has the strongest impact on the predicted GPP of the MOD17 algorithm (Wang et al., 2013). The assumption also is important because the overstory and understory could be decoupled from each other and would intercept different amounts of light and have different water sources during the growing season (Scott et al., 2003). Light quantity and quality as diffuse light or sunflecks determine differences among understorey species in their temporal response to gaps, involving acclimation and avoidance of photoinhibition (Pearcy, 2007). Another shortcoming is that few land cover classifications are incorporated into the MYD17 algorithm.

2.5 Santa Rita site dataset

Santa Rita Experimental Range (SRER) is located in the western range of the Santa Rita Mountains in Arizona, USA (31.8214 latitude, -110.8661 longitude, 1120 m asl.). Climate is BSk with mean annual precipitation of 380 mm, temperature of 17.9°C and Ustic Torri fluvents soils. Established in 1903, SRER has a long history of experimental manipulations to enhance grazing potential for cattle (Glenn et al., 2015). Two Ameriflux sites are located in the SRER: Santa Rita Grassland (US-SRG) and Santa Rita Mezquite (US-SRM). We used EC data for the years 2013-2019 from US-SRM which is a mesquite grass savanna (35% mesquite canopy cover and mean canopy height above 2m, 22% grasses and 43% bare soil), although MODIS describes this site as open shrublands (Glenn et al., 2015; Scott et al., 2004). The US-SRM site is dominated by velvet mesquite (*Prosopis velutina*), has a diversity of shrubs, cacti, succulents and bunch grasses (McClaran, 2003). This site was chosen because the vegetation and climate are similar to the Bernal site and it was the closest EC instrumentation with data availability (Figure 3).

Figure 3. Semidesert grassland encroached by mesquite (*Prosopis velutina*) at Santa Rita, Arizona (US-SRM). Image Credit: Russell Scott, 09/12/2016.

2.6 Modeling

Gross primary production estimated by EC at Bernal site was modeled using OLS and EML. The explanatory variables were the remote sensed data, the weather parameters and the vegetation indices (Appendix A). The OLS was fitted with the stepwise procedure, the final model included variables with a variance inflation factor (VIF) lower than 10 and a significance level of 0.05. Predictions of the EC GPP were obtained with the final model. Analysis and diagnostics were made with Minitab v 17 (Minitab LLC).

A stack of EML was obtained with the H2O package of R (H2O.ai 2017). This package provides several algorithms that can contribute to a stack of ensembles using the automl function: feedforward artificial neural network (DL), general linear models

(GLM), gradient boosting machine (GMB), extreme gradient boosting (XGBoost), default distributed random forest (DRF) and extremely randomized trees (XRT) and general linear models (GLM). Automl trains two stacked ensemble models, one ensemble contains all the models, and the second ensemble contains just the best performing model from each algorithm class/family; both of the ensembles should produce better models than any individual model from the automl run. The term automl (Automatic Machine Learning) implies data preprocessing, normalization, feature engineering, model selection, hyperparameter optimization, and prediction analysis; including procedures to identify and deal with non-independent and identically distributed observations and overfitting (Michailidis, 2018; Truong et al., 2019).

Machine learning has two elements for supervised learning: training loss and regularization. The task of training tries to find the best parameters for the model while minimizing the training loss function; the mean squared error for example. The regularization term controls the complexity of the model helping to reduce overfitting. Overfitting becomes apparent when the model performs accurately during the training but the accuracy is low during the testing. A good model needs extensive parameter tuning by running many times the algorithm to explore the effect on regularization and cross validation accuracy (Mitchell and Frank, 2017). In this investigation the function of training loss was the deviance, which is a generalization of the residual sum of squares driven by the likelihood. Deviance is a measure of model fit, lower or negative values indicate better model performance (McElreath, 2020).

A stack of EML solutions was based on a random sample of the dataset for training the model. For the Bernal site 85% was used for training and 80% in the case of US-SRM. The automl function was run 20 times, each run added approximately 48 models to the leaderboard and ranked the best performing models by their deviance. Each run splitted the training data ten times for k-fold cross-validation. The seed, for EML that is dependent on randomization, was changed in every run. The stopping rule for each run was set at 100 s and the maximum memory allocation pool for H2O was 100 Gb, in a single workstation with dual Xeon 2680 v4 processors and 128 Gb of RAM. The H2O package was installed in a rocker/geospatial docker container, which is a portable, scalable and reproducible environment (Boettiger and Eddelbuettel, 2017).

Two sets of predictions for the GPP at the Bernal site were obtained from the stacked ensemble. The first set of predictions was based on the 15% of the Bernal site data reserved for testing. The second set of predictions was obtained by re-feeding the US-SRM site model with the Bernal site explanatory variables. The first set of predictions would show the importance of local data to predict EC based GPP. The second set of predictions would represent the suitability of off-site data to predict EC based GPP. If the second scenario has good agreement, then an EML model could be used to represent wider areas of the ecosystem.

2.7 Model agreement

Stevens et al. (2017) proposes the probability of agreement (θs) as a plot-metric to represent the agreement between two measurement systems across a range of plausible values. Besides the agreement plot, agreement is based on maximum likelihood bias parameters: α and β quantifying the fixed bias and the proportional bias. If $\alpha=0$, $\beta=1$ and $\sigma 1 = \sigma 2$ then the two measurements are identical; where σj are the measurement variation. The probability of agreement analysis was performed using the ProbAgreeAnalysis (https://uwaterloo.ca/business-and-industrial-statistics-research-group/software) in Matlab 9.4

(MathWorks, Inc.). An arbitrary 1 g C m-2 d-1 was considered as a tolerable magnitude to conclude that agreement is sufficient as to use either estimate GPP interchangeably. The reference measurement was the GPP obtained from EC data at Bernal site and tested against the MODIS MOD17 model, the OLS predictions or each of the two sets of EML predictions. If the probability of agreement plot suggested disagreement between two measurement systems, then the predictions can be adjusted using:

$$Adjusted\ predictor = (predictor - \alpha)/\beta \quad \text{Eq. (4)}$$

2.8 Variable importance

The variable importance within individual models was used to answer the question of which environmental variables were important for GPP prediction. For the "all models ensemble" and "best of family ensemble" generated by automl is not possible to examine the variable importance nor the contribution of the individual models to the stack (H2O.ai 2017). Therefore, a weight (w_i) was calculated using equation (5), which is adequate for other information criterion besides the Akaike weights; this weight is an estimate of the conditional probability that the model will make best predictions on new data considering the set of models (McElreath, 2020). Then, the importance of each variable (%) was multiplied by the model's weight (w_i) and then added by variable to build the variable importance index. This index would measure how often a given variable was used in the leaderboard.

$$w_i = \frac{\exp\left(-\frac{1}{2} dWAIC_i\right)}{\sum_{j=1}^{m} \exp(-\frac{1}{2} dWAIC_i)} \quad \text{Eq. (5)}$$

$$dWAIC = deviance_i - deviance\ of\ top\ performing\ model \quad \text{Eq. (6)}$$

3 Results

Deserts and semi deserts comprise big areas and we need a way to represent their ecosystem functioning. If remote sensed data can be used to obtain similar results as those provided by instrumentations with eddy covariance (EC), then their relationship would be an initial step to upscaled representations. In this study, MODIS GPP had an acceptable agreement with GPP from EC data at the Bernal site, but an EML was better. However, the agreement of predictions made for Bernal using the best EML from Santa Rita and the environmental and remote sensed data from Bernal was not better than the MODIS estimates. Section 3.1 and 3.2 would present the details of model agreement for EML and MODIS respectively. In section 3.4 we present the EC flux time series and analysis indicating that the thorny scrub at Bernal was a carbon sink during the dry and the rainy seasons.

3.1 Machine learning ensembles as predictors of eddy covariance GPP

In this section we describe the modeling with EML using local remote sensed data from Bernal site to predict GPP at the same site, and then the agreement between EML GPP predictions and EC derived GPP. The automl function generated 1031 models

with an average deviance of 1.35 while the deviance of the leader model was 0.63 in the training data set (Table 1). Eleven models of type GBM and five models XGBoost were in the top 30 models, along with nine best of family ensembles and five all models ensembles. The weighted variable importance in the leaderboard was higher for the LAI from MOD13 and MCD13 products (17% and 14%). The PsnNet, EVI (MYD13), FPAR (MCD15), the green atmospherically resistance vegetation index (GARI) and MODIS reflectance band 13 had an importance higher than 3% (5.9, 5.4, 4.2, 3.6 and 3.0%). LAI (MCD13 and MOD13), PsnNet and the FPAR (MOD15) were the more important variables (20, 17, 13 and 10%) in the top non-staked model, a GBM model which was ranked in fourth place.

Predictions of GPP in the testing dataset showed dispersion in the lower range of the scale of measurement and the correlation was 0.94 (Figure 4A). The final prediction of GPP for the whole dataset had a probability of agreement (θs) of 0.58 ± 0.01 (parameter estimate and standard error), $\alpha = -0.0616 \pm 0.11$ and $\beta = 1.0133 \pm 0.02$, suggesting a good fit with low fixed and proportional bias (Figure 4B). The probability of agreement decreased slightly at the lower and upper range of the scale of measurement (Figure 4C), indicating that the EML model would predict GPP without increasing the bias, particularly in the range from 0 to 4 g C m^{-2} d^{-1}. However, the value of θs should be higher than 0.95 as to consider EC measurements and EML as interchangeable. The correlation of 0.99 ($r^2 = 0.98$) for the data in Fig. 4B could be misleading as it would suggest a very good fit.

Using only the five of the more important variables named above, to generate an EML, resulted in a XBoost leader model with 2.73 deviance and a total of 1094 models. Top 30 models were 16 XBoost and GBM models, and the best of family ensembles started to show up at the 12th place. Although the number of runs was the same (20), the automl function increased the number produced models; but the smaller set of explanatory variables constrained the ability to identify features contributing to better models. Using another set of five randomly selected explanatory variables (one vegetation index and four MODIS bands) resulted in a leader model with 2.52 deviance out of 1024 models, but this time the leader was the best of the family ensemble. Using only a few variables was considered to increase the deviance compared with the average deviance of 1.35 obtained during the training phase and using all available variables.

Table 1. Leaderboard of EML models for the Bernal training dataset consisting of 85% of day observations. NA denotes the outcome where the type of model was not present in the 30 top performing models, according to deviance.

Type of Model	**Number of models**	**Average deviance**		
		All models	**Top models**	**Leader model**
Stacked Ensemble				
All models	20	0.852	0.834	
Best of family	20	0.812	0.703	0.633

GBM	453	1.366	0.796
DRF	20	1.108	
XGBoost	277	1.385	0.778
XRT	20	1.077	
Deep Learning	201	2.072	
GLM	20	1.474	
Total	1031	1.356	

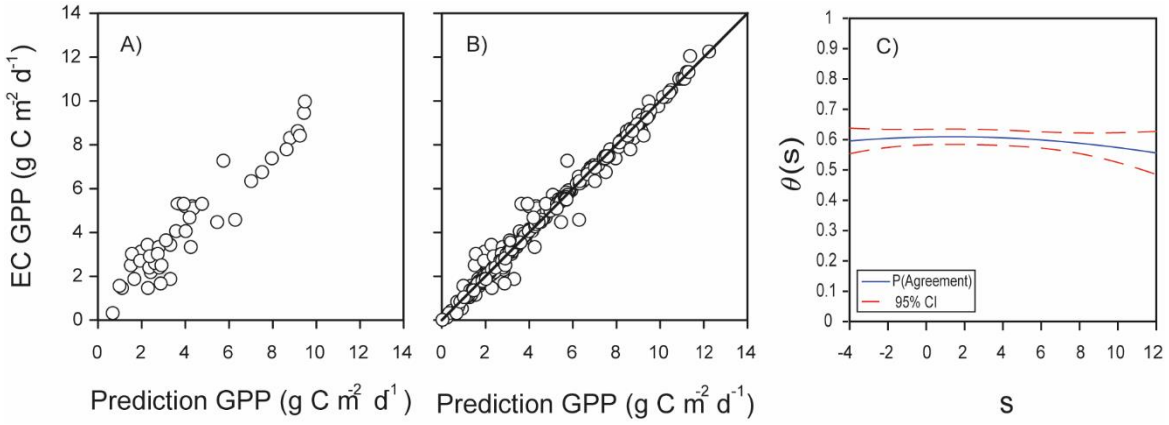

Figure 4. Agreement between predictions of GPP obtained with machine learning algorithms or derived from eddy covariance measurements at Bernal site. A) Example of one run predictions of GPP in the test dataset from Bernal site using the leader model of an ensemble of machine learning algorithms (EML), the test dataset was 15% of data, r= 0.94. B) Predictions for the complete dataset, r= 0.99, the diagonal line is the 1:1 agreement. C) Function of probability of agreement using a 1 g C m^{-2} d^{-1} as tolerable agreement between methods of estimation of GPP corresponding to plot B). The horizontal axis (s) represents the magnitude of the measurement, the vertical axis is the probability of agreement for the measurement, the red line is the confidence interval, $p < 0.05$.

An important question for modeling upscaling is the capacity to extrapolate results temporally and spatially; here we explored the latter posing the following question: predictions of GPP from EML for a EC site would agree with EC observations from another site with "similar" environmental conditions? First an EML solution was found training 80% of the Santa Rita dataset obtaining a best of family ensemble with 0.23 deviance out of 634 trained models. Then the environmental and remote sensed data from the Bernal site was fed into the model, this would be an external validation dataset. However, agreement was not good, the mean value of θs was 0.15 ± 0.01, α = -1.0822 ± 0.09 and β = 0.58127 ± 0.02. The value of θs was not constant across the range of measurement and decreased rapidly after 2 g C m^{-2} d^{-1} (Figure 5B). Because the bias was important the predictions were adjusted using equation (4), showing some improvement with r = 0.78 (Figure 5A). Comparing Fig. 4B and

5A it is evident that an EML model extrapolation to other conditions is noisier, ie. Santa Rita model trying to represent the ecosystem function at Bernal. Notwithstanding, some of the most important variables were shared by both EML ensembles: Bernal and Santa Rita; in the case of Santa Rita LAI from MOD15, MYD15 and MCD15 had 35.0, 4.8 and 3.1% of variable importance and for the FPAR from MOD15 was 12%.

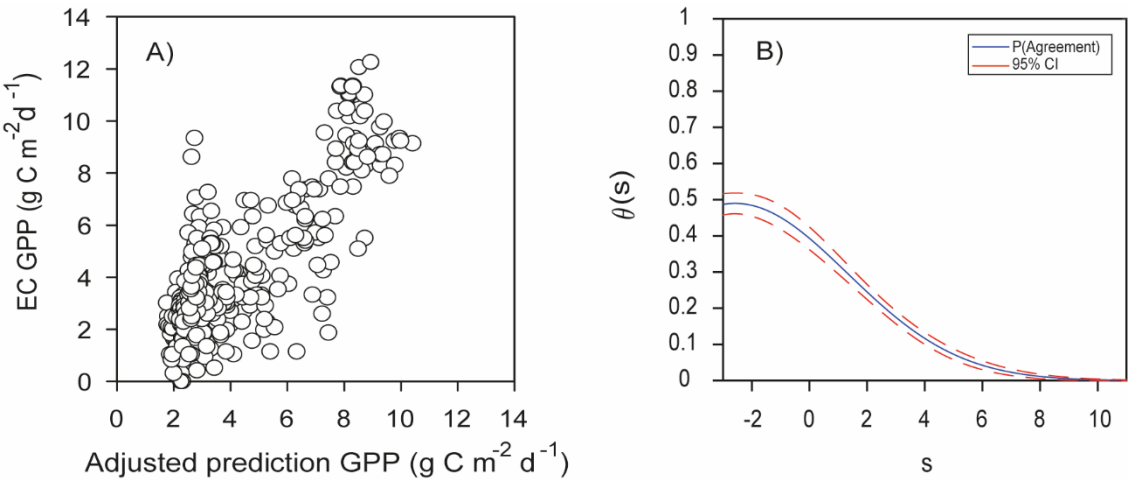

Figure 5. A) Adjusted predictions of GPP for the complete dataset from Bernal site using the leader model of the final ensemble of machine learning algorithms (EML) derived from Santa Rita site compared to estimates of GPP from EC data, r= 0.78. B) Respective function of probability of agreement using a 1 g C m^{-2} d^{-1} as tolerable agreement between methods of estimation of GPP: EC data from the Bernal site and EML model for the Santa Rita site. The horizontal axis (s) represents the magnitude of the measurement, the vertical axis is the probability of agreement for the measurement, the red line is the confidence interval, $p < 0.05$.

3.2 MODIS as predictor of eddy covariance GPP

MODIS is important because it overpases every point of the earth every one or two days and it implements a GPP product (MOD17) that has helped track the response of the biosphere to the environment since 2000. The product MOD17 has been validated against many EC sites, but few validation sites correspond to deserts and semi-deserts (Running et al., 2004). The GPP MOD17 underestimated the GPP derived from EC data at Bernal (Figure 6A). In a similar bell shaped distribution of θs, as in the case of the extrapolation of the Santa Rita site (Figure 5B), here the θs was not constant across the range of measurement; mean θs was 0.24 ± 0.13, $\alpha = 0.00047 \pm 0.087$ and $\beta = 0.48749 \pm 0.02$ (Figure 6C). Adjusting MOD17 estimates with equation (4) improved the relationship, but note that the value of r (0.76) was the same for original MOD17 and the adjusted MOD17 (Figure 6B).

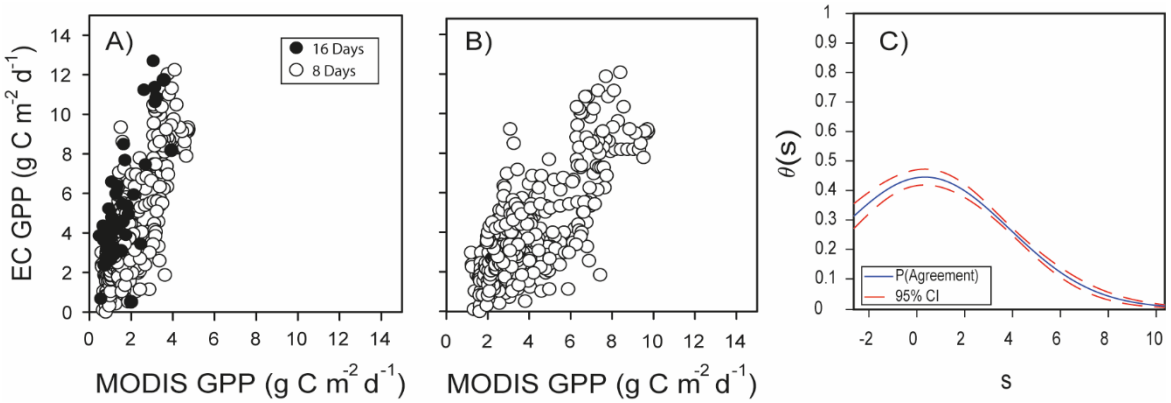

Figure 6. A) MODIS17 estimates of GPP from Bernal site versus estimates of GPP from EC data using the complete dataset at a daily time step derived from spline for MOD17 GPP (○), r= 0.76 or, eight-day composite estimates obtained by eight-day averages of EC GPP (●), r= 0.76. B) Adjusted predictions of GPP from MODIS. C) Respective function of probability of agreement using a 1 g C m^{-2} d^{-1} as tolerable agreement between methods of estimation of GPP: EC data from the Bernal site and MODIS MOD17. The horizontal axis (s) represents the magnitude of the measurement. The vertical axis is the probability of agreement for the measurement.

3.3 Prediction eddy covariance GPP with ordinary least squares multiple regression

OLS is a common estimation method for linear models and here this model appeared as adequate, judging by the general distribution of predictions (Figure 7A) and the probability of agreement plot (Figure 7B). Fourteen variables were included in the model, all of them with VIF values lower than 7.0 (Appendix B); the VIF statistic quantifies the severity of multicollinearity and an acceptable threshold is 10. The most significant variables were the EVI from MYD13 and Daymet variables precipitation, short wave radiation, and minimum and maximum temperatures (see Appendix A for variable details). Variables with high coefficient values were MODIS reflectance band 14 (9.17) the EVI from MYD13 (8.53), and the NDVI (3.9), while Daymet temperatures had small coefficients: -0.23 for maximum temperature and 0.17 for minimum temperature. The θs decreased slightly at the ends of the measurement range; mean θs was 0.5 ± 0.014, α = 0.18845 ± 0.137 and β = 0.94966 ± 0.031. No correction for this model was calculated since α was close to 0, β to 1 and the EML model had a higher θs.

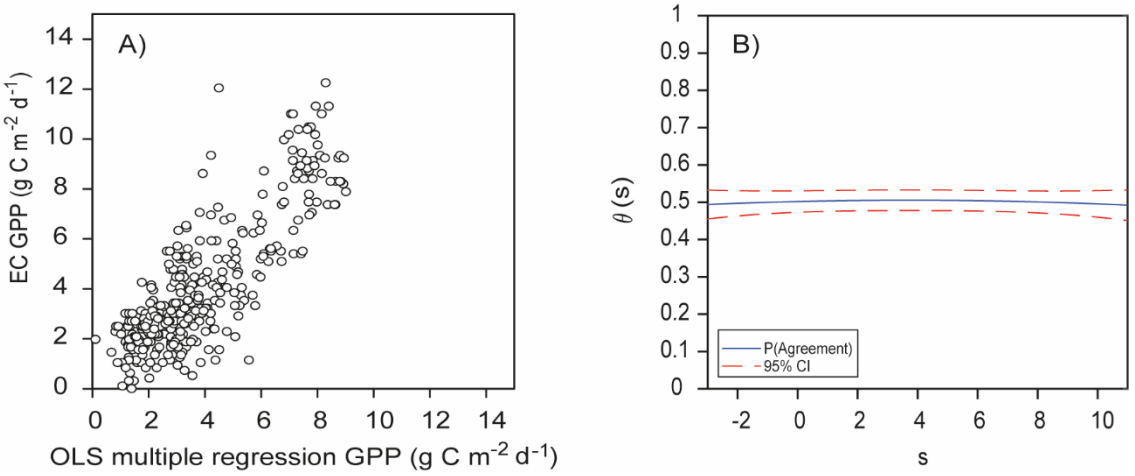

Figure 7. A) Ordinary least squares multiple regression estimates of GPP for the complete dataset from Bernal site versus estimates of GPP from EC data, r= 0.82. B) Respective function of probability of agreement using a 1 g C m^{-2} d^{-1} as tolerable agreement between methods of estimation of GPP: EC data from the Bernal site and OLS multiple regression. The horizontal axis (s) represents the magnitude of the measurement. The vertical axis is the probability of agreement for the measurement.

3.4 Eddy covariance fluxes at Bernal

Figure 8 shows energy balance closure for Bernal with a slope of 0.72 and $r^2 = 0.92$. Homogeneous sites of the Fluxnet network obtain higher percentages of closure than 72%, and for Bernal the site, the vegetation heterogeneity was important (see below). Average H was always negative during nighttime, but during some months of the dry and rainy season λE was positive, particularly after down (Figure 9), as to gurant nighttime evaporation from the soil or vegetation. However, during some months of the dry season rainfall was small (Figure 10), then the positive λE suggested that cacti could have an active gas exchange at that time.

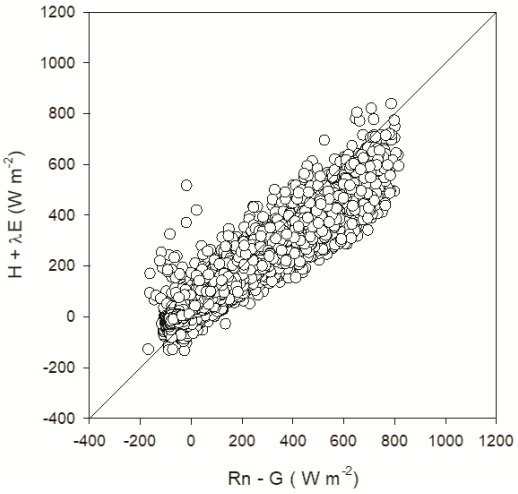

Figure 8. Closure of the surface energy balance from eddy covariance measurements averaged at 30 min between the turbulent fluxes (H+λE) and available fluxes (Rn-G). Data is from march 30, 2017 to august 22, 2018 at Bernal site. The regression was y = 23.02 + 0.72 x, adjusted r^2 = 0.92. Diagonal line represents the 1:1 relation.

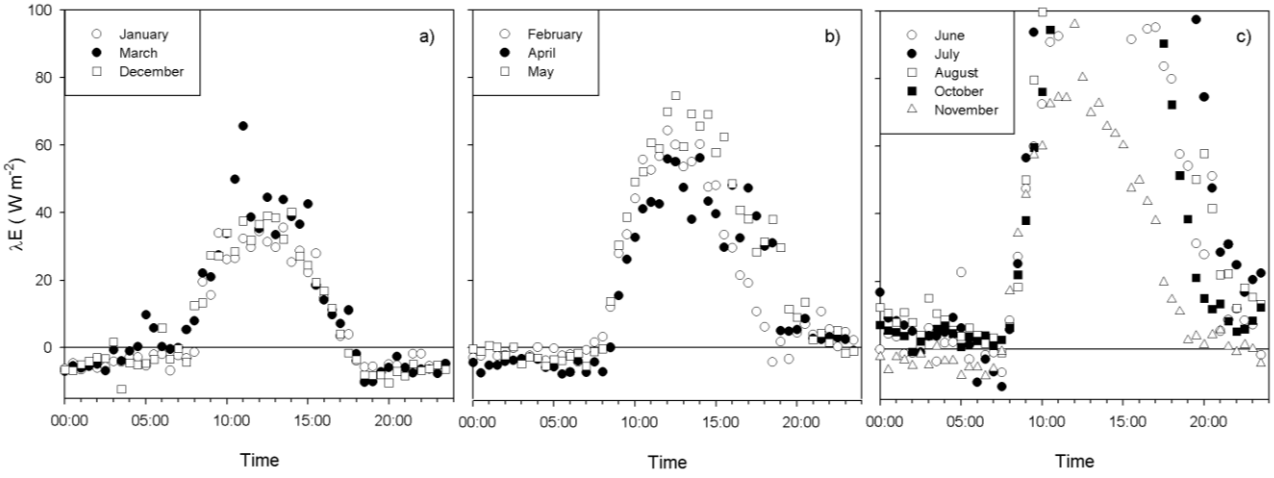

Figure 9. Latent heat flux daily trend at Bernal during different months emphasizing nighttime λE. A) shows months with low rainfall in the previous month and predominantly negative λE during nighttime (these months had low rainfall: 0.17, 11.3, 0.33 mm rainfall for January, March and December). B) shows months with low rainfall in the previous month and positive λE after sunset (6.7, 7.3, 20.7 mm rainfall for February, April and May). C) shows months during the rainy season with λE positive mainly due to soil wetness and antecedent rainfall of 43, 202, 9, 190, 34 mm for June, July, August, October and November. Plot C) is out of scale in the y axis for compatibility with the other plots.

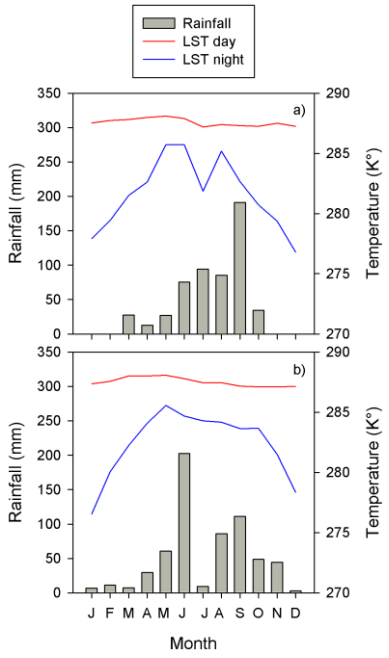

Figure 10. Monthly rainfall and land surface temperature (LST) during years, a) 2017 and b) 2018 at Bernal site. The LST values correspond to the 1:30 PM (LST day) and 1:30 AM (LST night) MODIS Aqua satellite overpasses.

Carbon dioxide absorptions had a diurnal behaviour beginning at dawn and ending before sunset (Figure 11). Nighttime flux was positive, indicating respiration, notwithstanding the presence of cacti. Although summer rains are characteristic of the climate at Bernal site (Figure 10), a negative NEE flux occurred at all measured months. The lowest CO_2 flux was recorded in January and February 2017 and in May 2018 (Table 2), this behaviour resulted from the phenology of the vegetation, since most species lost their leaves in the dry season, and also due to the effect of low temperature. Within the rainy season, the flux of CO_2 increased, compared to the months of January to June. The correlation between NEE and precipitation was -0.45. When the sum of the precipitation of the current month and that of the previous month was considered, the correlation with NEE was -0.7, suggesting that continuous availability of soil moisture is important for the absorption of CO_2 in this environment.

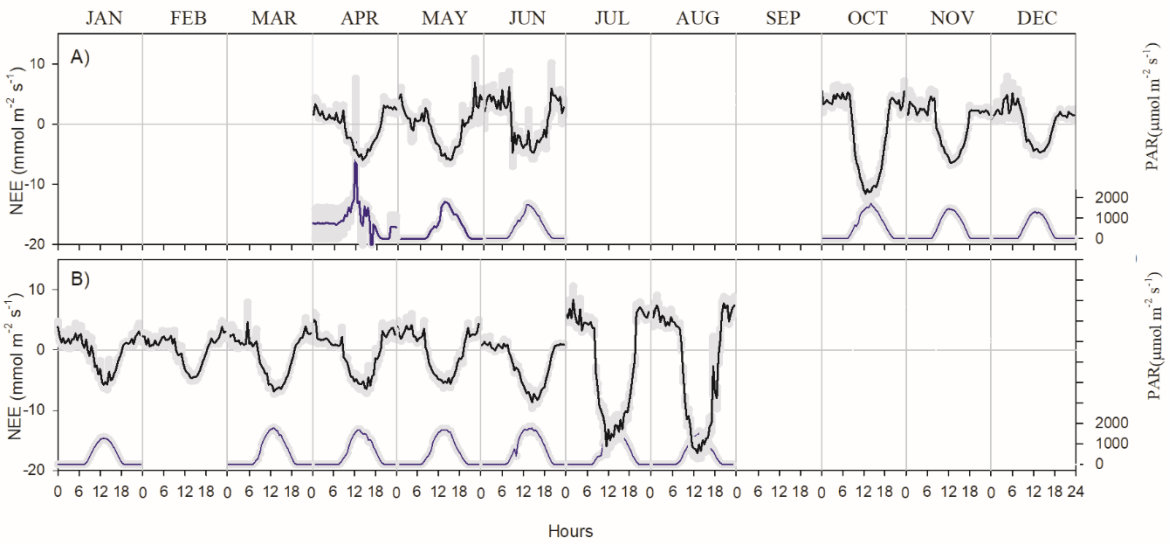

Figure 11. Net ecosystem exchange (NEE) and photosynthetic active radiation (PAR) at Bernal site in A) 2017 and B) 2018. Negative values in the CO_2 flux indicate photosynthesis. The grey shadow is the standard error of mean for each month at any given hour.

Table 2. Daily average values of the net ecosystem exchange (NEE), gross primary productivity (GPP), ecosystem respiration (R_{eco}) in a scrub at Bernal site. Negative values of NEE indicate photosynthetic absorption.

		NEE	GPP	R_{eco}
		µmol m^{-2} s^{-1}		
2017	JAN			
	FEB			
	MAR			
	APR	-0.54	2.48	1.94
	MAY	0.05	2.86	2.91
	JUN	0.38	4.21	4.59
	JUL	-1.00	1.78	0.77
	AGO			
	SEP			
	OCT	-1.26	5.25	3.99
	NOV	-0.13	2.65	2.52
	DEC	0.04	1.80	1.84
2018	JAN	-0.05	1.29	1.24
	FEB	0.06	1.88	1.94
	MAR	-0.94	2.45	1.51
	APR	-0.58	2.87	2.29

MAY	-0.29	3.77	3.48
JUN	-2.52	4.33	1.81
JUL	-2.83	8.23	5.41
AGO	-1.93	9.21	7.28

The scrub at Bernal was heterogeneous in botanical composition. Twenty-four species of cacti and shrub were identified; on average, each sampling plot had 10.3 species. The IVI was similar between all cacti (0.36 ± 0.04), shrub legumes (0.38 ± 0.04) and other shrubs (0.23 ± 0.06) sampled. *Cylindropuntia imbricata* had the largest IVI, followed by *Acacia farnesiana, Acacia schaffneri and Prosopis laevigata* (Table 3). The IVI of the herbaceous stratum represented by grasses was not characterized, due to the state of overgrazing and the absence of reproductive structures in plants, which made measurement difficult of their abundances, frequencies and dominances. The grass genera present were *Melinis*, *Chloris*, *Cynodon* and *Cenchrus*, corresponding all to invasive C_4 tropical grasses. Scrub species of higher IVI had a similar LAI (1.2), although the magnitude of the LAI of *P. laevigata* stood out (Table 3).

Table 3. Importance value index (IVI) and leaf area index (LAI) of the main species present at the Bernal, Querétaro study site.

Species	Plant type	IVI	SEM[1]	LAI	SEM
Coryphantha cornifera	Cactus	0.07	0.27		
Bouvardia ternifolia	Herb	0.07	0.27		
Karwinskia humboldtiana	Shrub	0.07	0.27		
Forestiera phillyreoides	Shrub	0.09	0.27		
Ferocactus latispinus	Cactus	0.09	0.27		
Cylindropuntia leptocaulis	Cactus	0.09	0.27		
Asphodelus fistulosus	Shrub	0.09	0.19		
Brickellia veronicifolia	Shrub	0.10	0.27		
Dalea lutea	Shrub	0.11	0.15		
Eysenhardtia polystachya	Legume	0.13	0.15		
Myrtillocactus geometrizans	Cactus	0.14	0.27		
Schinus molle	Shrub	0.14	0.19		
Jatropha dioica	Herb	0.15	0.19		
Mammillaria uncinata	Cactus	0.16	0.12		
Opuntia tomentosa	Cactus	0.17	0.11		
Opuntia robusta	Cactus	0.23	0.07		
Opuntia hyptiacantha	Cactus	0.26	0.07		

Mimosa monancistra	Legume	0.28	0.12		
Mimosa depauperata	Legume	0.31	0.12		
Zaluzania augusta	Shrub	0.33	0.10		
Viguiera linearis	Herb	0.36	0.11		
Acacia schaffneri	Legume	0.41	0.07	1.13	0.15
Prosopis laevigata	Legume	0.41	0.07	1.48	0.12
Acacia farnesiana	Legume	0.56	0.09	1.12	0.37
Cylindropuntia imbricata	Cactus	0.74	0.07	1.13	0.11

[1] SEM: standard error of the mean.

4 Discussion

4.1 Model agreement

Four approaches to estimate GPP were compared to predict GPP based on EC data. The probability of agreement (θs) was the statistic to determine if the mean responses were in agreement. Comparing the confidence intervals for θs the best modeling approach could be identified. The best result was the EML ensemble using environmental and remote sensed data corresponding to the same site, i.e. Bernal (Figure 4C). This EML would be useful for gap filling or the evaluation of GPP time series of the site that generated the model.

The second option to estimate GPP, using the same datasets, was the multiple regression OLS model (Figure 7A). The multiple regression is straightforward and here multicollinearity was not a problem. The EML ensemble and the OLS regression have the highest values of θs (0.58 and 0.5, respectively). Higher values for θs are desirable (>0.95) and this could be achieved by increasing the sample size, relaxing the tolerable magnitude for agreement (here was set at 1 g C m^{-2} d^{-1}), or perhaps using different forcing variables.

The MODIS estimates were a third best alternative, since the mean θs was 0.24. In the present study we used a spline to fill the data to a daily time step since the MCD17 is an eighth day composite product; but a similar result was obtained if the EC GPP was rescaled and compared to the original MCD17 data (Figure 6A). The GPP from MODIS was an underestimate of EC GPP and when the estimates were adjusted using equation (4) (Figure 6B) the performance was not better than the OLS (model not shown). The MODIS land cover classification represented this site as grassland (MCD12). Agreement of MODIS GPP is crucial because MODIS products are frequently used in country wide assessments of the carbon cycle and can influence public policies.

The model with least agreement resulted when the EML ensemble generated from the Santa Rita site used to predict GPP at Bernal. Machine learning models can make predictions but their usefulness decreases when they are used outside the context where they were built; while process based mechanistic models have this ability. The Santa Rita model was good at predicting

GPP at that site, with a deviance of the leader model of 0.23 while at Bernal the deviance of the leader model was 0.63 (Table 1), indicating that the Santa Rita EML ensemble was at least as good model as the EML at Bernal (not shown). The GPP time series for Santa Rita was about four times the size of the Bernal dataset and therefore the deviance was lower. However, when the Santa Rita model was used with Bernal data the mean θs was 0.16, indicating that the agreement was insufficient. Eyeballing the predictions in Figures 5A, 6B and 7A and their corresponding correlation values (0.78, 0.76 and 0.82 for adjusted EML Santa Rita, adjusted MODIS and multiple regression OLS) it could be argued that these models were comparable. However, their θs plots present a different perspective.

4.2 MODIS discrepancies

Different authors have reported discrepancies between MCD17 and EC estimates of GPP in semi-arid regions; examining MODIS discrepancies in these ecosystems is important because the errors induced by cloud cover are expected to be minimal and other effects can be identified (Gebremichael and Barros, 2006). The GPP of MOD17 did not relate well (EC = 0.11 + 0.17 MODIS, $r^2 = 0.67$) with estimates of EC GPP in semi-desert vegetation of Sahel (Tagesson et al., 2017). With data from different types of vegetation in the Heihe basin in China, MODIS17 overestimated the GPP from EC (EC = 1.15 + 0.24 MODIS, $r^2 = 0.68$, Cui et al., 2016). For scrub sites in Mexico, the relation between GPP calculated from EC and MOD17 was not good (MODIS = 383.82 + 0.467 EC, $r^2 = 0.6$, (Delgado-Balbuena et al., 2018). In arid and semi-arid ecosystems in China, optimizing parameters of the MODIS GPP model with site-specific data, improved the estimate to explain 91% of the variation in the GPP of the data observed by EC (Wang et al., 2019). These same authors propose improving the land use classification used by the MOD17 algorithm and recalibrating light use efficiency parameters to solve the GPP estimation problem. Gebremichael and Barros (2006) examined an open shrubland site in a semi-arid region of Sonora, Mexico and their analysis of the temporal evolution of the discrepancies with MODIS GPP suggested revisiting the light use efficiency parameterization, especially the functional dependence on VPD and PAR and water stress or soil moisture availability.

The relationship between the GPP MODIS and the GPP EC presented in section 3.2 is an approximation, because the uncertainty in the respiration component must be considered. The empirical relationship between nocturnal NEE and soil temperature has been used to represent ecosystem respiration (R_{eco}) in order to separate the processes that contribute to daytime NEE(Richardson and Hollinger, 2005; Wofsy et al., 1993). Nighttime NEE should be equal to the rates of autotrophic and heterotrophic respiration, while during daytime, NEE should be equal to the combined rates of carboxylation and oxidation of RUBISCO, autotrophic respiration and heterotrophic respiration. Then the GPP can be calculated as the difference between daytime NEE and R_{eco}, estimated through its relationship with temperature (Goulden et al., 1996). In the present study, R_{eco} was calculated based on soil/air temperature following the procedure of Reichstein et al. (2005) implemented in Reddyproc (Wutzler et al., 2018). Although it is possible to measure or model the partition of respiration (Running et al., 2004; Wang et al., 2018), the presence of cacti complicates, assuming that all nighttime flux represents ecosystem respiration (Owen et al., 2016; Richardson and Hollinger, 2005). While soil respiration tends to be temperature-limited when soil moisture is non-limiting in temperate ecosystems, in rangeland ecosystems the controls of soil CO_2 efflux were photosynthesis, soil temperature

and moisture (Roby et al., 2019). In our study, the instrumentation did not include measurements of plant or soil respiration partition to validate the R_{eco} estimates.

A problem regarding data comparison from remote orbital sensors and terrestrial observations is that different quantities are fundamentally measured. MODIS measures the radiation reflected by the earth's surface in two spectral bands at 250 m spatial resolution per pixel, five bands at 500 m and 29 bands at 1 000 m. The EC technique has a footprint to measure CO_2 that varies dynamically in shape and size, but is generally considered to be 1 km². To solve the scaling, MODIS products related to the carbon cycle have been validated with the EC technique and biometric measurements on several spatial scales using process-based ecosystem models and characterizing areas up to 47 km^2 around the EC measuring tower (Cohen et al., 2003).

At Bernal the vegetation was heterogeneous, this situation was represented by the heterogeneity in vegetation activity in the four pixels used; ranging about 0.2 units of NDVI at the peak of the season activity (Figure 1). The standard error of the IVI differed by one order of magnitude among species. Although more important species had a lower standard error; but their means were similar indicating that they were equally abundant at all sampling plots. The higher importance of some species (Table 3) was explained by selective grazing-browsing behaviour and the dispersion caused by cattle, either by ingesting or transporting seeds or plant parts (Belayneh and Tessema, 2017). Regarding landscape heterogeneity, the tower fetch was predominantly from the northeast, capturing the less heterogeneous area of the site but also the more active, according to the NDVI (Figure 1).

The thorny scrub examined had two vegetation layers: the overstory layer mainly consisting of mesquite, acacia and cacti, and the understory layer that included grasses and herbs. Cattle preferentially graze the understory and because they eat using their tongue they will avoid browsing thorny species, unlike goats or deer that use their lips. Without grazing management, overtime, the competition balance will favour bush species resulting in encroaching and the understory will be stressed; only unpalatable species or those with their growing meristems very close to the ground would survive. Representing the structure and functioning of these two layers using MODIS is possible (Liu et al., 2017). Recently, Hill and Guerschman (2020) presented a MODIS product derived from MCD43A4 to estimate the fractions of photosynthetic and non-photosynthetic vegetation and the remaining fraction of bare soil. These developments could improve the MOD17 GPP estimates, since its model represents a homogeneous single vegetation layer. All these considerations help to understand the low θs between MOD17 estimates of GPP and EC derived GPP.

4.3 Carbon flux

Although the carbon balance in ecosystems is influenced by different factors such as soil type and amount of nutrients, the relationship with soil temperature and humidity is particularly strong (Anderson-Teixeira et al., 2011; Hastings et al., 2005). How much of the rainwater the system can retain or lose has been described as the leakiness of the system (Guerschman et al., 2009). More than immediate incident rainfall, the available soil moisture and its redistribution are important in semi-arid ecosystems, including steamflow, preferential flow paths, hydraulic lift and others (Barron-Gafford et al., 2017). At Bernal, when the sum of the precipitation of the current month and that of the previous month was considered, the correlation with

NEE was -0.7, suggesting that continuous availability of soil moisture is important for the absorption of CO_2 in this environment. This result is consistent with other studies in which the relationship between the net productivity of the ecosystem (NEP) and precipitation is initially positive, but is levelled from 1000 to 1500 mm annually (Xu et al., 2014). The hydraulic redistribution of water from moist (deeper) to drier soils through plant roots tended to increase modeled annual ecosystem uptake of CO_2, this process was identified at US-SMR (Fu et al., 2018; Scott et al., 2003).

The leakiness is highly dependent upon vegetation fractional cover, the proportion of the surface occupied by bare soil and vegetation: photosynthetically active vegetation and non-photosynthetically active vegetation such as litter, wood and dead biomass (Guerschman et al., 2009). It is possible that the canopy of the bushes completely intercepted the rainfall in some months, because the scrub can intercept up to 20% of the precipitation and its canopy storage capacity is 0.97 mm (Mastachi-Loza et al., 2010). Considering only the daily rain events greater than 5 mm, the correlation between precipitation and NEE rose to -0.72. In the present study, the interception of rain by vegetation surfaces was not calculated, but the results suggest that it would be important to explore the relationship between net precipitation and NEE.

The average NEE at a global level is -156 ± 284 g C m^{-2} y^{-1} (Baldocchi, 2014). The highest frequency among sites that measured NEE with EC occurs from 200 to 300 g C m^{-2} y^{-1}, but in sites with biometric measurements, the peak occurs at 100 g C m^{-2} y^{-1} (Xu et al., 2014). Using the daily averages of Table 2, the average NEE during the measurement period was -0.78 g C m^{-2} d^{-1} and annually would be -283.5 g C m^{-2} y^{-1}. This result was higher than the annual values of the induced grassland and scrubland vegetation characterizing the Sonora desert plains (138 and 130 g C m^{-2} y^{-1}, Hinojo-Hinojo et al., 2019). In New Mexico, NEE values measured with EC are between 35-50 g C m^{-2} y^{-1} in desert grassland and 344-355 g C m^{-2} y^{-1} in mixed coniferous forest (Anderson-Teixeira et al., 2011). In a dryer region, the sarcocaulescent scrubland of Baja California in Mexico, the NEE was -39 and -52 g C m^{-2} y^{-1} in 2002 and 2003, respectively (Hastings et al., 2005). The NEE measured here was within the range of NNE 0.3 ± 0.2 kg C m^{-2} yr^{-1} for grasslands/shrublands in Mexico (Murray-Tortarolo et al., 2016). Although the measurements of the present study had gaps and were compared with annual studies, we considered that the reported value of C was representative of the main season of growth of this type of scrub.

4.4 Final remarks

Overgrazing is an appreciation relative to the grazing productive system where the forage resource is overused; in a mixed shrub-grass ecosystem, such as Bernal, usually refers to the understory. Overgrazing means that the plant regrowth is readily grazed, tillers and root reserves are lost and eventually the plant may die. Although the Bernal site was overgrazed, the carbon fluxes indicated that the plant community was photosynthetically active in both the dry and rainy seasons. It is fair to assume that the water in the soil was not limiting for the deep rooted bush species and that was the reason why it was possible to maintain the photosynthetic function during rainless months. However, this primary production would not have tangible benefits for rancher's production system, since no edible biomass would be produced for the cattle. From the point of view of carbon capture, the system accumulated non-labile biomass that would remain in the system for a longer time compared to a

grassland ecosystem (although it would be necessary to determine the partition of said shrub biomass). However, the overgrazing condition affects the biomass of the understory roots and consequently the carbon pool in the soil.

In the short term, it can be thought that the estimated negative carbon flows are a favourable effect on the environmental agenda. As time passes, it is possible that the gaps between the individual shrubs of the overstory expand and this would have had an effect on soil erosion. It is also possible that the water stored in the soil profile used by the bushes gradually decreases, to the point of causing drought, changes in phenology and advancing the desertification process. There are many opportunities for ecology conservation and livestock-oriented management; this may include controlled grazing or propagating native thornless shrub species. If the ranchers do not identify a benefit in the vegetation, then they will be tempted to remove it, as it occurred at the study site. Because of its wide coverage and readily availability the MODIS GPP product, accuracy is important in representing the carbon cycle, raising awareness and monitoring advancement of environmental decisions.

Although we found that the EML was a good option for modeling the GPP of a site, what is really needed to evaluate the performance of semiarid ecosystems is a spatial representation of the carbon flux. This is a problem for an underrepresented area regarding instrumented EC towers. However, the EML could be designed to take into account the explanatory variables in a spatiotemporal continuity. As demonstrated here, extrapolating the EML model from one site to another had poor agreement.

5 Conclusion

The Bernal site was a carbon sink notwithstanding its overgrazed condition. This is due to the contribution to the carbon flux of the predominating shrub species in this area. The probability of agreement between EC derived GPP and remote sensed estimates of GPP for the study site was acceptable at 0.6 when using a machine learning ensemble; linear multiple regression had a 0.5 probability of agreement. For these two methods the probability of agreement was uniform across the range of measurement. Gross primary production estimates from MODIS had a probability of agreement of 0.24 and this probability decreased rapidly with increasing values of GPP. Although the importance value index of cacti was high in the study area, their metabolic activity did not outweigh the respiration component of the CO_2 flux during nighttime; therefore, it is necessary to measure autotrophic and heterotrophic respiration components of the ecosystem. Precipitation was related to NEE but the soil water balance must be studied because the growing season of this vegetation type extends well beyond the predominant summer monsoon.

Data availability

Database and programming code are available at https://doi.org/10.5281/zenodo.3598595

Author contribution

Guevara-Escobar contributed to conceptualization, formal analysis, investigation, methodology, software, supervision, validation, visualization, writing – original draft and review & editing.

E. González-Sosa was in charge of funding acquisition, project administration and writing – review.

M. Cervantes-Jimenez contributed to investigation, methodology, validation, visualization, writing – original draft and review, editing and communication.

M. E. Queijeiro-Bolaños helped with investigation, validation, writing – review.

H. Suzán-Azpiri contributed with conceptualization and writing – review.

I. Carrillo- Ángeles helped with investigation and writing – review.

V. H. Cambrón-Sandoval contributed with writing – review and funding acquisition.

Competing interest

The authors declare that they have no conflict of interest.

Acknowledgments

The work was financially supported by CONACyT - SEMARNAT project no. 2014-1-(249407). Data filtering was carried out by the cluster Abacus I, Centre of Applied Mathematics and High Performance Computing ABACUS-CINVESTAV.

References

Aguirre-Díaz, G. J., Aguillón-Robles, A., Tristán-González, M., Labarthe-Hernández, G., López-Martínez, M., Bellon, H. and Nieto-Obregón, J.: Geologic setting of the Peña de Bernal Natural Monument, Querétaro, México: An endogenous volcanic dome, Geosphere, 9(3), 557–571, doi:10.1130/GES00843.1, 2013.

Anav, A., Friedlingstein, P., Beer, C., Ciais, P., Harper, A., Jones, C., Murray-Tortarolo, G., Papale, D., Parazoo, N. C. and Peylin, P.: Spatiotemporal patterns of terrestrial gross primary production: A review, Rev. Geophys., 53(3), 785–818, doi:https://doi.org/10.1002/2015RG000483, 2015.

Anderson-Teixeira, K. J., Delong, J. P., Fox, A. M., Brese, D. A. and Litvak, M. E.: Differential responses of production and respiration to temperature and moisture drive the carbon balance across a climatic gradient in New Mexico, Glob. Change Biol., 17(1), 410–424, doi:https://doi.org/10.1111/j.1365-2486.2010.02269.x, 2011.

Baldocchi, D.: Measuring fluxes of trace gases and energy between ecosystems and the atmosphere–the state and future of the eddy covariance method, Glob. Change Biol., 20(12), 3600–3609, doi:https://doi.org/10.1111/gcb.12649, 2014.

Barron-Gafford, G. A., Sanchez-Cañete, E. P., Minor, R. L., Hendryx, S. M., Lee, E., Sutter, L. F., Tran, N., Parra, E., Colella, T., Murphy, P. C., Hamerlynck, E. P., Kumar, P. and Scott, R. L.: Impacts of hydraulic redistribution on grass–tree competition vs facilitation in a semi-arid savanna, New Phytol., 215(4), 1451–1461, doi:10.1111/nph.14693, 2017.

Belayneh, A. and Tessema, Z. K.: Mechanisms of bush encroachment and its inter-connection with rangeland degradation in semi-arid African ecosystems: a review, J. Arid Land, 9(2), 299–312, doi:https://doi.org/10.1007/s40333-016-0023-x, 2017.

Bickford, C. P.: Ecophysiology of leaf trichomes, Funct. Plant Biol., 43(9), 807–814, doi:https://doi.org/10.1071/FP16095, 2016.

Boettiger, C. and Eddelbuettel, D.: An introduction to rocker: Docker containers 639 for r, ArXiv Prepr. ArXiv171003675, 640, 2017.

Bonilla-Moheno, M. and Aide, T. M.: Beyond deforestation: Land cover transitions in Mexico, Agric. Syst., 178, 102734, doi:https://doi.org/10.1016/j.agsy.2019.102734What can ecological science tell us about opportunities for carbon sequestration on arid rangelands in the United States?, 2020.

Booker, K., Huntsinger, L., Bartolome, J. W., Sayre, N. F. and Stewart, W.: What can ecological science tell us about opportunities for carbon sequestration on arid rangelands in the United States?, Glob. Environ. Change, 23(1), 240–251, doi:https://doi.org/10.1016/j.gloenvcha.2012.10.001, 2013.

Butzer, K. W. and Butzer, E. K.: The 'natural'vegetation of the Mexican Bajío: archival documentation of a 16th-century savanna environment, Quat. Int., 43, 161–172, doi:https://doi.org/10.1016/S1040-6182(97)00032-3, 1997.

CICESE, C. de I. C. y de E. S. de E.: Base de datos climatológica nacional (CLICOM)., Villa Bernal, Querétaro. [online] Available from: http://clicom-mex.cicese.mx/ (Accessed 28 August 2019), 2015.

Cui, T., Wang, Y., Sun, R., Qiao, C., Fan, W., Jiang, G., Hao, L. and Zhang, L.: Estimating vegetation primary production in the Heihe River Basin of China with multi-source and multi-scale data, PloS One, 11(4), 1–20, doi:https://doi.org/10.1371/journal.pone.0153971, 2016.

Curtis, J. T. and McIntosh, R. P.: The Interrelations of Certain Analytic and Synthetic Phytosociological Characters, Ecology, 31(3), 434–455, doi:10.2307/1931497, 1950.

Delgado-Balbuena, J., Yepez, E. A., Ángeles-Pérez, G., Aguirre-Gutierrez, C., Arredondo, T., Ayala-Niño, F., Bullock, S. H., Castellanos, A. E., Cueva, A., Figueroa-Espinoza, B., Garatuza-Payán, J., Hinojo-Hinojo, C., Maya-Delgado, Y., Méndez-Barroso, L., Oechel, W., Paz-Pellat, F., Pérez-Ruíz, E. R., Rodríguez, J. C., Rojas-Robles, N., Sánchez-Mejía, Z. M., Uuh-Sonda, J., Vargas, R., Verduzco, V. S., Vivoni, E. R. and Watts, C.: Flujos anuales de carbono en ecosistemas terrestres de México, in Estado Actual del Conocimiento del Ciclo del Carbono y sus Interacciones en México: Síntesis a 2018., p. 686, Texcoco, Estado de México, México., 2018.

Eshel, G., Dayalu, A., Wofsy, S. C., Munger, J. W. and Tziperman, E.: Listening to the Forest: An Artificial Neural Network-Based Model of Carbon Uptake at Harvard Forest, J. Geophys. Res. Biogeosciences, 124(3), 461–478, doi:10.1029/2018JG004791, 2019.

Fu, C., Wang, G., Bible, K., Goulden, M. L., Saleska, S. R., Scott, R. L. and Cardon, Z. G.: Hydraulic redistribution affects modeled carbon cycling via soil microbial activity and suppressed fire, Glob. Change Biol., 24(8), 3472–3485, doi:10.1111/gcb.14164, 2018.

Gebremichael, M. and Barros, A. P.: Evaluation of MODIS Gross Primary Productivity (GPP) in tropical monsoon regions, Remote Sens. Environ., 100(2), 150–166, doi:10.1016/j.rse.2005.10.009, 2006.

Gilles, J. L. and Jamtgaard, K.: Overgrazing in pastoral areas: The commons reconsidered, Nomadic Peoples, 1–10, doi:https://doi.org/10.1111/j.1467-9523.1981.tb00298., 1982.

Gitelson, A. A., Peng, Y., Arkebauer, T. J. and Suyker, A. E.: Productivity, absorbed photosynthetically active radiation, and light use efficiency in crops: Implications for remote sensing of crop primary production, J. Plant Physiol., 177, 100–109, doi:https://doi.org/10.1016/j.jplph.2014.12.015, 2015.

Glenn, E. P., Scott, R. L., Nguyen, U. and Nagler, P. L.: Wide-area ratios of evapotranspiration to precipitation in monsoon-dependent semiarid vegetation communities, J. Arid Environ., 117, 84–95, doi:10.1016/j.jaridenv.2015.02.010, 2015.

Goldstein, A., Turner, W. R., Spawn, S. A., Anderson-Teixeira, K. J., Cook-Patton, S., Fargione, J., Gibbs, H. K., Griscom, B., Hewson, J. H. and Howard, J. F.: Protecting irrecoverable carbon in Earth's ecosystems, Nat. Clim. Change, 1–9, doi:https://doi.org/10.1038/s41558-020-0738-8, 2020.

Goulden, M. L., Munger, J. W., Fan, S., Daube, B. C. and Wofsy, S. C.: Measurements of carbon sequestration by long-term eddy covariance: Methods and a critical evaluation of accuracy, Glob. Change Biol., 2(3), 169–182, doi:https://doi.org/10.1111/j.1365-2486.1996.tb00070.x, 1996.

Green, J. K., Konings, A. G., Alemohammad, S. H., Berry, J., Entekhabi, D., Kolassa, J., Lee, J.-E. and Gentine, P.: Regionally strong feedbacks between the atmosphere and terrestrial biosphere, Nat. Geosci., 10(6), 410–414, doi:https://doi.org/10.1038/ngeo2957, 2017.

Guerschman, J. P., Hill, M. J., Renzullo, L. J., Barrett, D. J., Marks, A. S. and Botha, E. J.: Estimating fractional cover of photosynthetic vegetation, non-photosynthetic vegetation and bare soil in the Australian tropical savanna region upscaling the EO-1 Hyperion and MODIS sensors, Remote Sens. Environ., 113(5), 928–945, doi:10.1016/j.rse.2009.01.006, 2009.

Hansen, J., Sato, M., Hearty, P., Ruedy, R., Kelley, M., Masson-Delmotte, V., Russell, G., Tselioudis, G., Cao, J. and Rignot, E.: Ice melt, sea level rise and superstorms: evidence from paleoclimate data, climate modeling, and modern observations that 2° C global warming is highly dangerous., Atmospheric Chem. Phys. Discuss., 15(14), doi:https://doi.org/10.5194/acp-16-3761-2016, 2015.

Hastings, S. J., Oechel, W. C. and Muhlia-Melo, A.: Diurnal, seasonal and annual variation in the net ecosystem CO2 exchange of a desert shrub community (Sarcocaulescent) in Baja California, Mexico, Glob. Change Biol., 11(6), 927–939, doi:https://doi.org/10.1111/j.1365-2486.2005.00951.x, 2005.

Henrich, V., Krauss, G., Götze, C. and Sandow, C.: Entwicklung einer Datenbank für Fernerkundungsindizes, vol. 45, Bochum., 2012.

Hill, M., Held, A., Leuning, R., Coops, N., Hughes, D. and Cleugh, H.: MODIS spectral signals at a flux tower site: Relationships with high-resolution data, and CO2 flux and light use efficiency measurements, Remote Sens. Environ., 103(3), 351–368, doi:https://doi.org/10.1016/j.rse.2005.06.015, 2006.

Hill, M. J. and Guerschman, J. P.: The MODIS Global Vegetation Fractional Cover Product 2001–2018: Characteristics of Vegetation Fractional Cover in Grasslands and Savanna Woodlands, Remote Sens., 12(3), 406, doi:10.3390/rs12030406, 2020.

Hinojo-Hinojo, C., Castellanos, A. E., Huxman, T., Rodriguez, J. C., Vargas, R., Romo-León, J. R. and Biederman, J. A.: Native shrubland and managed buffelgrass savanna in drylands: Implications for ecosystem carbon and water fluxes, Agric. For. Meteorol., 268, 269–278, doi:https://doi.org/10.1016/j.agrformet.2019.01.030, 2019.

Järvi, L., Havu, M., Ward, H. C., Bellucco, V., McFadden, J. P., Toivonen, T., Heikinheimo, V., Kolari, P., Riikonen, A. and Grimmond, C. S. B.: Spatial modeling of local-scale biogenic and anthropogenic carbon dioxide emissions in Helsinki, J. Geophys. Res. Atmospheres, 124(15), 8363–8384, doi:https://doi.org/10.1029/2018JD029576, 2019.

Jung, M., Schwalm, C., Migliavacca, M., Walther, S., Camps-Valls, G., Koirala, S., Anthoni, P., Besnard, S., Bodesheim, P., Carvalhais, N., Chevallier, F., Gans, F., Groll, D. S., Haverd, V., Ichii, K., Jain, A. K., Liu, J., Lombardozzi, D., Nabel, J. E. M. S., Nelson, J. A., Pallandt, M., Papale, D., Peters, W., Pongratz, J., Rödenbeck, C., Sitch, S., Tramontana, G., Weber, U., Reichstein, M., Koehler, P., O'Sullivan, M. and Walker, A.: Scaling carbon fluxes from eddy covariance sites to globe: Synthesis and evaluation of the FLUXCOM approach, Biogeosciences Discuss., 2019, 1–40, doi:10.5194/bg-2019-368, 2019.

Lal, R., Griffin, M., Apt, J., Lave, L. and Morgan, M. G.: Managing Soil Carbon, Science, 304(5669), 393–393, doi:10.1126/science.1093079, 2004.

Lightfoot, D. C.: The effects of livestock grazing and climate variation on vegetation and grasshopper communities in the northern Chihuahuan Desert, J. Orthoptera Res., 35–51, 2018.

Liu, Y., Liu, R., Pisek, J. and Chen, J. M.: Separating overstory and understory leaf area indices for global needleleaf and deciduous broadleaf forests by fusion of MODIS and MISR data, Biogeosciences, 14(5), 1093–1110, doi:https://doi.org/10.5194/bg-14-1093-2017, 2017.

Long, S. P., Marshall-Colon, A. and Zhu, X.-G.: Meeting the Global Food Demand of the Future by Engineering Crop Photosynthesis and Yield Potential, Cell, 161(1), 56–66, doi:10.1016/j.cell.2015.03.019, 2015.

Ma, X., Huete, A., Yu, Q., Restrepo-Coupe, N., Beringer, J., Hutley, L. B., Kanniah, K. D., Cleverly, J. and Eamus, D.: Parameterization of an ecosystem light-use-efficiency model for predicting savanna GPP using MODIS EVI, Remote Sens. Environ., 154, 253–271, 2014.

Ma, X., Migliavacca, M., Wirth, C., Bohn, F. J., Huth, A., Richter, R. and Mahecha, M. D.: Monitoring Plant Functional Diversity Using the Reflectance and Echo from Space, Remote Sens., 12(8), 1248, doi:https://doi.org/10.3390/rs12081248, 2020.

Males, J.: Think tank: water relations of Bromeliaceae in their evolutionary context, Bot. J. Linn. Soc., 181(3), 415–440, doi:https://doi.org/10.1111/boj.12423, 2016.

Marcolla, B., Rödenbeck, C. and Cescatti, A.: Patterns and controls of inter-annual variability in the terrestrial carbon budget, Biogeosciences, 14(16), 3815–3829, doi:doi:10.5194/bg-14-3815-2017, 2017.

Mastachi-Loza, C. A., González-Sosa, E., Becerril-Piña, R. and Braud, I.: Pérdidas por intercepción en mezquite (Prosopis laevigata) y huizache (Acacia farnesiana) de la región semiárida del centro de México, Tecnol. Cienc. Agua, 1(1), 103–120, 2010.

Mauder, M. and Foken, T.: Documentation and instruction manual of the eddy-covariance software package TK3, 2011.

McClaran, M.: A century of vegetation change on the Santa Rita Experimental Range In Santa Rita Experimental Range: one-hundred years (1903-2003) of accomplishments and contributions Ed, RMRSUS Dep. Agric. For. Serv. Ogden UT, 197, 2003.

McCulley, R., Jobbagy, E., Pockman, W. and Jackson, R.: Nutrient uptake as a contributing explanation for deep rooting in arid and semi-arid ecosystems, Oecologia, 141(4), 620–628, doi:http://dx.doi.org/10.1007/s00442-004-1687-z, 2004.

McElreath, R.: Statistical Rethinking: A Bayesian Course with Examples in R and STAN, CRC Press., 2020.

Medrano, F. G.: Las zonas áridas y semiáridas de México y su vegetación, Instituto Nacional de Ecología., 2012.

Michailidis, M.: How Driverless AI Prevents Overfitting and Leakage, Open Source Lead. AI ML [online] Available from: https://www.h2o.ai/blog/driverless-ai-prevents-overfitting-leakage/ (Accessed 7 July 2020), 2018.

Mirzabaev, A., Wu, J., Evans, J., Garcia-Oliva, F., Hussein, I. A. G., Iqbal, M. H., Kimutai, J., Knowles, T., Meza, F., Nedjroaoui, D., Tena, F., Türkeş, M., Vázquez, R. J. and Weltz, M.: Desertification, in Climate Change and Land: an IPCC special report on climate change, desertification, land degradation, sustainable land management, food security, and greenhouse gas fluxes in terrestrial ecosystems, edited by P. R. Shukla, J. Skeg, E. Calvo Buendia, V. Masson-Delmotte, H.-O. Pörtner, D. C. Roberts, P. Zhai, R. Slade, S. Connors, S. van Diemen, M. Ferrat, E. Haughey, S. Luz, M. Pathak, J. Petzold, J. Portugal Pereira, P. Vyas, E. Huntley, K. Kissick, M. Belkacemi, and J. Malley., 2019.

Mitchell, R. and Frank, E.: Accelerating the XGBoost algorithm using GPU computing, PeerJ Comput. Sci., 3, e127, doi:https://doi.org/10.7717/peerj-cs.127, 2017.

Monteith, J.: Solar radiation and productivity in tropical ecosystems, J. Appl. Ecol., 9(3), 747–766, 1972.

Murray-Tortarolo, G., Friedlingstein, P., Sitch, S., Jaramillo, V. J., Murguía-Flores, F., Anav, A., Liu, Y., Arneth, A., Arvanitis, A., Harper, A., Jain, A., Kato, E., Koven, C., Poulter, B., Stocker, B. D., Wiltshire, A., Zaehle, S. and Zeng, N.: The carbon cycle in Mexico: past, present and future of C stocks and fluxes, Biogeosciences, 13(1), 223–238, doi:https://doi.org/10.5194/bg-13-223-2016, 2016.

Owen, N. A., Choncubhair, Ó. N., Males, J., del Real Laborde, J. I., Rubio-Cortés, R., Griffiths, H. and Lanigan, G.: Eddy covariance captures four-phase crassulacean acid metabolism (CAM) gas exchange signature in Agave, Plant Cell Environ., 39(2), 295–309, doi:https://doi.org/10.1111/pce.12610, 2016.

Pasetto, D., Arenas-Castro, S., Bustamante, J., Casagrandi, R., Chrysoulakis, N., Cord, A. F., Dittrich, A., Domingo-Marimon, C., El Serafy, G. and Karnieli, A.: Integration of satellite remote sensing data in ecosystem modelling at local scales: Practices and trends, Methods Ecol. Evol., 9(8), 1810–1821, doi:https://doi.org/10.1111/2041-210X.13018, 2018.

Pearcy, R. W.: Heterogeneous light environments, in Handbook of Functional Plant Ecology, pp. 270–314, CRC Press, FL, USA., 2007.

Piao, S., Liu, Q., Chen, A., Janssens, I. A., Fu, Y., Dai, J., Liu, L., Lian, X., Shen, M. and Zhu, X.: Plant phenology and global climate change: Current progresses and challenges, Glob. Change Biol., 25(6), 1922–1940, doi:https://doi.org/10.1111/gcb.14619, 2019.

R Development Core Team: R: A language and environment for statistical computing. R Foundation for Statistical Computing, [online] Available from: https://www.r-project.org (Accessed 15 October 2015), 2009.

Reichstein, M., Falge, E., Baldocchi, D., Papale, D., Aubinet, M., Berbigier, P., Bernhofer, C., Buchmann, N., Gilmanov, T. and Granier, A.: On the separation of net ecosystem exchange into assimilation and ecosystem respiration: review and improved algorithm, Glob. Change Biol., 11(9), 1424–1439, doi:https://doi.org/10.1111/j.1365-2486.2005.001002.x, 2005.

Richardson, A. D. and Hollinger, D. Y.: Statistical modeling of ecosystem respiration using eddy covariance data: maximum likelihood parameter estimation, and Monte Carlo simulation of model and parameter uncertainty, applied to three simple models, Agric. For. Meteorol., 131(3–4), 191–208, doi:https://doi.org/10.1016/j.agrformet.2005.05.008, 2005.

Richardson, A. D., Hollinger, D. Y., Shoemaker, J. K., Hughes, H., Savage, K. and Davidson, E. A.: Six years of ecosystem-atmosphere greenhouse gas fluxes measured in a sub-boreal forest, Sci. Data, 6(1), 1–15, doi:https://doi.org/10.1038/s41597-019-0119-1, 2019.

Roby, M. C., Scott, R. L., Barron-Gafford, G. A., Hamerlynck, E. P. and Moore, D. J. P.: Environmental and Vegetative Controls on Soil CO2 Efflux in Three Semiarid Ecosystems, Soil Syst., 3(1), 6, doi:10.3390/soilsystems3010006, 2019.

Running, S. W. and Zhao, M.: Daily GPP and annual NPP (MOD17A2/A3) products NASA Earth Observing System MODIS land algorithm, MOD17 User's Guide, 2015, 2015.

Running, S. W., Nemani, R. R., Heinsch, F. A., Zhao, M., Reeves, M. and Hashimoto, H.: A continuous satellite-derived measure of global terrestrial primary production, Bioscience, 54(6), 547–560, doi:https://doi.org/10.1641/0006-3568(2004)054[0547:ACSMOG]2.0.CO;2, 2004.

Rzedowski, J.: Vegetación de México: México, Editor. Limusa, 1978.

Sarukhán, J., Urquiza-Haas, T., Koleff, P., Carabias, J., Dirzo, R., Ezcurra, E., Cerdeira-Estrada, S. and Soberón, J.: Strategic actions to value, conserve, and restore the natural capital of megadiversity countries: the case of Mexico, BioScience, 65(2), 164–173, doi:https://doi.org/10.1093/biosci/biu195, 2015.

Scott, R. L., Watts, C., Payan, J. G., Edwards, E., Goodrich, D. C., Williams, D. and James Shuttleworth, W.: The understory and overstory partitioning of energy and water fluxes in an open canopy, semiarid woodland, Agric. For. Meteorol., 114(3), 127–139, doi:10.1016/S0168-1923(02)00197-1, 2003.

Scott, R. L., Edwards, E. A., Shuttleworth, W. J., Huxman, T. E., Watts, C. and Goodrich, D. C.: Interannual and seasonal variation in fluxes of water and carbon dioxide from a riparian woodland ecosystem, Agric. For. Meteorol., 122(1), 65–84, doi:10.1016/j.agrformet.2003.09.001, 2004.

Scott, R. L., Biederman, J. A., Hamerlynck, E. P. and Barron-Gafford, G. A.: The carbon balance pivot point of southwestern US semiarid ecosystems: Insights from the 21st century drought, J. Geophys. Res. Biogeosciences, 120(12), 2612–2624, 2015.

Segerstrom, K.: Geology of the Bernal-Jalpan Area, Estado de Queretaro, Mexico, Geol. Surv. Bull., 1104, 19–82, 1961.

Soper, F. M., McCalley, C. K., Sparks, K. and Sparks, J. P.: Soil carbon dioxide emissions from the Mojave desert: Isotopic evidence for a carbonate source, Geophys. Res. Lett., 44(1), 245–251, doi:https://doi.org/10.1002/2016GL071198, 2017.

Spracklen, D., Baker, J., Garcia-Carreras, L. and Marsham, J.: The effects of tropical vegetation on rainfall, Annu. Rev. Environ. Resour., doi:https://doi.org/10.1146/annurev-environ-102017-030136, 2018.

Stevens, N. T., Steiner, S. H. and MacKay, R. J.: Assessing agreement between two measurement systems: An alternative to the limits of agreement approach, Stat. Methods Med. Res., 26(6), 2487–2504, doi:10.1177/0962280215601133, 2017.

Tang, Q., Vivoni, E. R., Muñoz-Arriola, F. and Lettenmaier, D. P.: Predictability of evapotranspiration patterns using remotely sensed vegetation dynamics during the North American monsoon, J. Hydrometeorol., 13(1), 103–121, doi:https://doi.org/10.1175/JHM-D-11-032.1, 2012.

Thornton, P., Thornton, M., Mayer, B., Wei, Y., Devarakonda, R., Vose, R. and Cook, R.: Daymet: Daily Surface Weather Data on a 1-km Grid for North America, Version 3. ORNL DAAC, USA, 2017.

Truong, A., Walters, A., Goodsitt, J., Hines, K., Bruss, C. B. and Farivar, R.: Towards automated machine learning: Evaluation and comparison of automl approaches and tools, pp. 1471–1479, IEEE., 2019.

Wang, H., Li, X., Ma, M. and Geng, L.: Improving estimation of gross primary production in dryland ecosystems by a model-data fusion approach, Remote Sens., 11(3), 225, doi:https://doi.org/10.3390/rs11030225, 2019.

Wang, X., Ma, M., Li, X., Song, Y., Tan, J., Huang, G., Zhang, Z., Zhao, T., Feng, J. and Ma, Z.: Validation of MODIS-GPP product at 10 flux sites in northern China, Int. J. Remote Sens., 34(2), 587–599, doi:https://doi.org/10.1080/01431161.2012.715774, 2013.

Wang, X., Wang, H., Li, X. and Ran, Y.: Photosynthesis (NPP, NEP, Respiration), Obs. Meas. Ecohydrol. Process., 1–30, doi:https://doi.org/10.1007/978-3-662-47871-4_10-2, 2018.

Wheeler, C. W., Archer, S. R., Asner, G. P. and McMurtry, C. R.: Climatic/edaphic controls on soil carbon/nitrogen response to shrub encroachment in desert grassland, Ecol. Appl., 17(7), 1911–1928, doi:https://doi.org/10.1890/06-1580.1, 2007.

Wilcox, B. P., Birt, A., Fuhlendorf, S. D. and Archer, S. R.: Emerging frameworks for understanding and mitigating woody plant encroachment in grassy biomes, Curr. Opin. Environ. Sustain., 32, 46–52, doi:10.1016/j.cosust.2018.04.005, 2018.

Wilson, J. B.: Cover plus: ways of measuring plant canopies and the terms used for them, J. Veg. Sci., 22(2), 197–206, doi:https://doi.org/10.1111/j.1654-1103.2010.01238.x, 2011.

Wofsy, S., Goulden, M., Munger, J., Fan, S.-M., Bakwin, P., Daube, B., Bassow, S. and Bazzaz, F.: Net exchange of CO2 in a mid-latitude forest, Science, 260(5112), 1314–1317, doi:https://doi.org/10.1126/science.260.5112.1314, 1993.

Wu, C., Niu, Z. and Gao, S.: Gross primary production estimation from MODIS data with vegetation index and photosynthetically active radiation in maize, J. Geophys. Res. Atmospheres, 115(D12), doi:https://doi.org/10.1029/2009JD013023, 2010.

Wutzler, T., Lucas-Moffat, A., Migliavacca, M., Knauer, J., Sickel, K., Šigut, L., Menzer, O. and Reichstein, M.: Basic and extensible post-processing of eddy covariance flux data with REddyProc, Biogeosciences, 15(16), 5015–5030, doi:https://doi.org/10.5194/bg-15-5015-2018, 2018.

Xiao, H., McDonald-Madden, E., Sabbadin, R., Peyrard, N., Dee, L. E. and Chadès, I.: The value of understanding feedbacks from ecosystem functions to species for managing ecosystems, Nat. Commun., 10(1), 1–10, doi:https://doi.org/10.1038/s41467-019-11890-7, 2019.

Xu, B., Yang, Y., Li, P., Shen, H. and Fang, J.: Global patterns of ecosystem carbon flux in forests: A biometric data-based synthesis, Glob. Biogeochem. Cycles, 28(9), 962–973, doi:https://doi.org/10.1002/2013GB004593, 2014.

Yao, J., Liu, H., Huang, J., Gao, Z., Wang, G., Li, D., Yu, H. and Chen, X.: Accelerated dryland expansion regulates future variability in dryland gross primary production, Nat. Commun., 11(1), 1–10, doi:https://doi.org/10.1038/s41467-020-15515-2, 2020.

Yepez, E. A., Williams, D. G., Scott, R. L. and Lin, G.: Partitioning overstory and understory evapotranspiration in a semiarid savanna woodland from the isotopic composition of water vapor, Agric. For. Meteorol., 119(1–2), 53–68, doi:https://doi.org/10.1016/S0168-1923(03)00116-3, 2003.

Yona, L., Cashore, B., Jackson, R. B., Ometto, J. and Bradford, M. A.: Refining national greenhouse gas inventories, Ambio, 1–6, doi:https://doi.org/10.1007/s13280-019-01312-9, 2020.

Zeng, X., Zeng, X. and Barlage, M.: Growing temperate shrubs over arid and semiarid regions in the Community Land Model–Dynamic Global Vegetation Model, Glob. Biogeochem. Cycles, 22(3), doi:https://doi.org/10.1029/2007GB003014, 2008.

Zhang, A., Jia, G., Epstein, H. E. and Xia, J.: ENSO elicits opposing responses of semi-arid vegetation between Hemispheres, Sci. Rep., 7, 42281, doi:https://doi.org/10.1038/srep42281, 2017.

Zhang, L., Xiao, J., Zheng, Y., Li, S. and Zhou, Y.: Increased carbon uptake and water use efficiency in global semi-arid ecosystems, Environ. Res. Lett., 15(3), 034022, doi:https://doi.org/10.1088/1748-9326/ab68ec, 2020.

Zhu, X.-G., Long, S. P. and Ort, D. R.: What is the maximum efficiency with which photosynthesis can convert solar energy into biomass?, Curr. Opin. Biotechnol., 19(2), 153–159, doi:https://doi.org/10.1016/j.copbio.2008.02.004, 2008.

Appendix A

Table A1. MODIS reflectance bands and products database.

Product name	Satellite layer	Spatial resolution	Temporal resolution (days)	Spectral coverage (nm)
MOD09GA	Band1	500 m	1	620-670
	Band2			841-876
	Band3			459-479
	Band4			545-565
	Band5			1230-1250
	Band6			1628-1652
	Band7			2105-2155
MODOCGA	Band8	1 km		405-420
	Band9			438-448
	Band10			483-493
	Band11			526-536
	Band12			546-556
	Band13			662-672
	Band14			673-683
MOD17A2H	Gross Primary Production (GPP)		8	N/A
	Net Photosynthesis (PsnNet)			
MOD15A2H	Fraction of Photosynthetically Active Radiation (Fpar)			
	Leaf Area Index (LAI)			
MOD11A2	Land Surface Temperature and Emissivity of day (LST day)	1 km		
	Land Surface Temperature and Emissivity of night (LST night)			

Table A1. MODIS reflectance bands and products database. (Continuation)

Product name	Satellite layer	Spatial resolution	Temporal resolution (days)	Spectral coverage (nm)
MYD13A1	Enhanced Vegetation Index (EVI)	500 m	16	N/A
MYD15A2H	Fraction of Photosynthetically Active Radiation (Fpar) Leaf Area Index (LAI)		8	
MYD11A2	Land Surface Temperature and Emissivity of day (LST day) Land Surface Temperature and Emissivity of night (LST night)	1 km		
MCD15A2H	Fraction of Photosynthetically Active Radiation (Fpar) Leaf Area Index (LAI)	500 m		

Table A2. Daily vegetation indexes computed using the MODIS reflectance bands described in Table 1.

Index	Formula	Reference
Simple Ratio (SimpleR)	$SimpleR = \frac{Band2}{Band1}$	
Moisture Stress (MoistS)	$MoistS = \frac{Band6}{Band2}$	
Disease Stress Index (DSI)	$DSI = \frac{Band2 + Band4}{Band6 + Band1}$	(Hill *et al.*, 2006)
Red Green Ratio Index (RGRI)	$RGRI = \frac{Band1}{Band4}$	
Normalized Difference Vegetation Index (NDVI)	$NDVI = \frac{Band2 - Band1}{Band2 + Band1}$	
Normalized Difference Water Index (NDVI_w)	$NDVI_{\_w} = \frac{Band2 - Band5}{Band2 + Band5}$	
Green Leaf Index (GLI)	$GLI = \frac{2 * Band11 - Band14 - Band9}{2 * Band11 + Band14 + Band}$	
Green Atmospherically Resistance Vegetation (GARI)	$GARI = \frac{Band5 - (Band11 - (Band9 - Band14))}{Band5 - (Band11 + (Band9 - Band14))}$	(Henrich *et al.*, 2012)
Enhanced Vegetation Index (EVI)	$EVI = 2.5 * \frac{Band2 - Band1}{Band2 + (6 * Band1) - (7.5 * Band9) + 1}$	

Table A3. Daymet meteorological database.

Variable	Spatial resolution	Temporal resolution	Reference
Precipitation (Dayprc) Shortwave radiation (Daysrad) Maximum air temperature (DayTmax) Minimum air temperature (DayTmin) Water vapor pressure (Dayvp)	1 km	Daily	(Thornton et al., 2017)

Table A4. Precipitation data.

Satellite	Product name	Spatial resolution	Temporal resolution
Global Precipitation Measurement (GPM)	3IMERGDF v006	0.1 Degree	Daily
Tropical Rainfall Measuring Mission (TRMM)	3B42 v007	0.25 Degree	

Appendix B

Table B1. Analysis of variance for GGP derived from EC data at Bernal site. Variable details are described in Appendix A.

Model term	Coefficient	EE[1]	DF[2]	SC[3]	F	p	VIF[4]
Regression			14	1780.48			
Constant	-13.18	6.48			-2.03	0.043	
R_08_405.420[5]	-2.119	0.602	1	26.8	-3.52	0	2.2
R_13_662.672[5]	-2.86	1.23	1	11.61	-2.32	0.021	1.55
R_14_673.683[5]	9.17	2.59	1	27.06	3.53	0	1.22
RGRI[6]	-0.832	0.369	1	11	-2.25	0.025	1.43
GARI[6]	2.01	1.08	1	7.55	1.87	0.063	2.37
EVIMYD[7]	8.53	2.01	1	39.03	4.25	0	2.94
NDVI_w[6]	3.9	1.55	1	13.67	2.51	0.012	2.71
PsnNet[7]	0.01312	0.00223	1	75.3	5.9	0	3.83
LstNgtMYD[7]	0.0462	0.0238	1	8.18	1.94	0.053	2.01
Davprc[8]	0.1388	0.0341	1	35.9	4.07	0	1.92
Davsrad[8]	0.0106	0.00218	1	51.21	4.86	0	5.01
DavTmax[8]	-0.2386	0.0581	1	36.58	-4.11	0	6.89
DavTmin[8]	0.1752	0.0454	1	32.22	3.86	0	4.96
TRMM$_9$	-0.0434	0.0194	1	10.87	-2.24	0.026	1.41
Error			403	872.97			
Total			417	2653.45			

1 Standard error of coefficient.

2 Degrees of freedom.

3 Adjusted sum of squares.

4 Variance inflation factor.

5 Variable name denotes the band number and spectral bandwidth of MODIS (Moderate Resolution Imaging Spectroradiometer).

6 Vegetation indices RGRI is red green ratio index: and GARI is green atmospherically resistance vegetation index, details of formula are described in Appendix I.

7 Layers from MODIS products. EVIMYD is enhanced vegetation index from MYD13

PsnNet is photosynthesis product form MOD17, LstNgtMYD is nighttime land surface temperature emissivity from MYD11.

8 Variables obtained from Daymet daily dataset: DayTmin is minimum temperature, DayTmax is maximum temperature, Daysrad is shortwave radiation, Dayprc is precipitation.

4 Daily rainfall rate from 3B42 TRMM (Tropical Rainfall Measuring Mission).